Materials Today Chemistry 26 (2022) 101176

Contents lists available at ScienceDirect

Materials Today Chemistry

journal homepage: www.journals.elsevier.com/materials-today-chemistry/

Synthesis of a biocompatible benzophenone-substituted chitosan hydrogel as novel coating for PEEK with extraordinary strong antibacterial and anti-biofilm properties

M. Borgolte [a, b], O. Riester [a, c], I. Quint [a, c], F. Blendinger [d, e], V. Bucher [d], S. Laufer [c, f], R. Csuk [b], L. Scotti [g], H.-P. Deigner [a, h, i, *]

[a] Institute of Precision Medicine, Furtwangen University, Jakob-Kienzle Str. 17, 78054 Villingen-Schwenningen, Germany
[b] Martin-Luther University Halle-Wittenberg, Organic Chemistry, Kurt-Mothes-Str. 2, 06120, Halle, Saale, Germany
[c] Institute of Pharmaceutical Sciences, Department of Pharmacy and Biochemistry, Eberhard-Karls-University Tuebingen, Auf der Morgenstelle 8, Tuebingen, 72076, Germany
[d] Institute for Microsystems Technology (iMST), Furtwangen University, Neckartal 142, Rottweil, 78628, Germany
[e] Institute for Applied Physics, Eberhard Karls University Tuebingen, Auf der Morgenstelle 8, Tübingen, 72076, Germany
[f] Tuebingen Center for Academic Drug Discovery & Development (TüCAD2), Tübingen, 72076, Germany
[g] Department of Medical, Oral and Biotechnological Sciences, University "G. D'Annuzio" of Chieti-Pescara, Via Dei Vestini, 66100, Chiety, Italy
[h] Faculty of Science, Eberhard Karls University Tuebingen, Auf der Morgenstelle 8, Tübingen, 72076, Germany
[i] EXIM Department, Fraunhofer Institute IZI (Leipzig), Schillingallee 68, 18057, Rostock, Germany

ARTICLE INFO

Article history:
Received 17 May 2022
Received in revised form
10 August 2022
Accepted 28 August 2022
Available online xxx

Keywords:
Chitosan
UV-Crosslinker
Antimicrobial coating
Anti-biofilm coating
Biocompatible

ABSTRACT

Chitosan derivatives substituted with benzophenone groups that can be cross-linked by ultraviolet light were synthesized as coatings for PEEK substrates used in the construction of lumbar cages. The IC_{90} values of the benzophenone-modified chitosan polymers in solution before crosslinking were in the same range as those reported for native chitosan. The resulting hydrogel surface after crosslinking exhibited excellent antimicrobial properties and was highly effective (up to 5 log-fold) against clinically relevant strains of methicillin-resistant *S. aureus* and *E. coli*. As a result, the coated surface also significantly reduced biofilm formation. The coatings show good biocompatibility with numerous cell lines as well as low levels of cytotoxicity (ISO 10993−5) and pyrogenicity (ISO 10993−11). The coatings also exhibited strong antioxidant properties toward formed hydroxyl radicals in an in-vitro Fenton reaction. Overall, substitution of chitosan with benzophenone residues is an interesting and important approach to the functionalization of materials used for medical implants that are prone to microbial contamination and mechanical failure. Biocompatible antimicrobial coatings might also be employed in photopatterning methods used in the design of medical devices.

1. Introduction

Chitosan is the deacetylated derivative of chitin that exhibits antimicrobial properties due to the positive charge of the amino groups of its constituent glucosamines. Due to this cationic properties, chitosan is able to disrupt the outer and inner bacterial cell membrane [1–4], via interactions of its polycationic properties with the negatively charged phosphocholine groups of the bacterial cell wall as suggested by the Shai-Matsuzaki-Huang (SMH) model of the behavior of cationic antimicrobial peptides in solution, leading to the antimicrobial properties of chitosan as well [5,6]. This is backed by a publication from Li et al., 2010, who investigated *E. coli* after chitosan treatment under an electron microscope, finding partly cell lysis and dissolved cell membranes of *E. coli* [7]. Another publication, analyzing an experimental chitosan coating, showed cell lysis and cytosol leakage of *S. epidermis* on the substrate [8]. As second potential mechanism, chitosan has been proposed to bind DNA inside the bacterial cytosol, inhibiting mRNA synthesis and therefore, inhibiting microbial growth and biofilm formation. This ability also follows the electrostatic interaction model, proposed by the SMH model, but refers to shorter chained chitosan molecules, which are able to penetrate the cell wall. A

* Corresponding author.
E-mail address: dei@hs-furtwangen.de (H.-P. Deigner).

https://doi.org/10.1016/j.mtchem.2022.101176

study on *E. coli* using fluorescein-modified chitosan, analyzed with a confocal laser microscope, shows an accumulation of chitosan inside the bacteria [9]. A third proposed mechanism of chitosan is based on its metal chelating ability [10]. Through this chelating ability free Ca^{2+} and Mg^{2+} cations, present in the bacterial cell wall, are bound, leading to decreased enzyme activity in the cell wall and,therefore, inhibition and disruption of bacterial growth [1,11–14]. In all cases, the bacteria are disturbed in their metabolism upon contact with the coated chitosan surface and, therefore, ultimately killed and unable to biofilm formation.

Due to these unique antimicrobial properties, several publications describe the use of chitosan for its antimicrobial properties in medicine-related applications. For example, thiolated mucoadhesive chitosan fibers prevent the growth of bacteria that cause dental caries while exhibiting no cytotoxicity against relevant cell lines [15]. Similarly, chitosan limits the formation of biofilms of *Actinobacillus pleuromoniae* [16]. Findings reported in another recent publication revealed that the introduction of chitosan *N*-halamine conjugates in hemostatic wound dressings resulted in a one million-fold reduction in the extent of microbial contamination [17]. Other applications for chitosan that have been widely described in the literature include bone tissue engineering [18-20], stem cell encapsulation [21–23], and wound dressings [24,25]. Unmodified chitosan has only limited solubility in both aqueous and organic solvents and exhibits comparatively poor mechanical properties and heat resistance. Thus, the use of chitosan as an antimicrobial coating for medical implants remains limited. However, the aforementioned studies revealed that chitosan may serve as an attractive substrate for specific functionalization designed to improve its properties and use on implant surfaces prone to microbial infection.

Benzophenone is a UV-responsive crosslinker, described in several publications over the last 30 years regarding photopatterning, including the generation of surface-anchored benzophenone hydrogels that promote cell adhesion [26–28] and micropatterning for analytical purposes [28–31] as well as for the design of antimicrobial and anti-adhesive surfaces [26,32–35]. We recently published a description of the synthesis of a benzophenone-acrylamide hydrogel in which *N*-acetyl glucosamine units were connected by various oligoethylene glycol chains. This hydrogel was used successfully to prevent microbial growth and biofilm formation when used as a coating for polyethylene terephthalate glycol (PETG) coverslips [36]. The mechanism of the underlying crosslinking reaction has been extensively reviewed [37-40]. Briefly, by activation through photons, benzophenone forms a highly reactive triplet radical via n-π^* or π-π^* transition, while the exact orbital transition depends on the wavelength [41]. This transition of a nonbonding n orbital of the oxygen into the π^*-LUMO of the carbonyl group leads to a biradicaloid state of the benzophenone. The then formed electrophilic ketyl radical can abstract a hydrogen atom from a nearby substrate or polymer chain, leading to two alkyl radicals, undergoing recombination, and therefore, crosslinking [42]. The kinetics of such C–H crosslinking reactions, leading to surface-anchored polymer networks and their surface-bond gelling kinetics, have also been described by Rühe et al. **2016**, showing unique, non-linear kinetics of the crosslinking reaction inside the coating hydrogel network [43].

Functionalization of glycosidic polymers with benzophenone has been described primarily for the design of UV-protective scaffolds. For example, Heo et al. [44] described the modification of pullulan with benzophenone that exhibited UV-absorption properties while maintaining good biocompatibility, thereby suggesting its use in the formulations of sunscreens [38]. Similarly, Morimoto et al. [38] described the synthesis of UV-absorbing phenolic chitosan derivatives with formaldehyde in a Mannich reaction [37]. Likewise, Hong et al. [45] described the antimicrobial activity of benzophenone-modified cotton; in this case, benzophenone functioned as an antimicrobial agent after UV irradiation and radical activation [45].

Polyether ether ketone (PEEK) is a high-performance thermoplastic, showing similar mechanical properties like the Ti6Al4V titanium alloy which is commonly used in medical applications [46] and displaying properties similar to human bone [47]. It is not cytotoxic, nor does it degrade or leach ions into the surrounding tissue [48]. Given these properties, it has been used for manufacturing of a variety of medical implants, for example, spinal cages [49–52], endoprotheses for hip replacement [53–55], or implants for cranial reconstructions [56,57] which can also be manufactured in a 3D printing process [58–61]. Given its otherwise bioinert surface, tissue integration and osseointegration of PEEK is still an issue of concern, leading to the need of proper surface functionalization of PEEK implants [62]. Therefore, multiple approaches for surface functionalization have been described, for example, deposition of inorganic substrates via atomic layer deposition (ALD) [63]. Newer works aim at further improving the mechanical properties of PEEK, for example by blending with other polymers and incorporation of carbon fibers [64] or calcium hydroxyapatite together with graphene [65]. A newer approach focusses on polydopamine coating on PEEK, able to complex Ca^{2+} ions in order to improve biocompatibility and bone mineralisation on the PEEK surface [66]. Since the PEEK consists of a diphenyl ketone group, similar to those present in benzophenone, this functional group is able to undergo the same radical generation mechanism via the n-π^* transition induced by UV light as used with benzophenone, [67]. Further, it been employed as radical starter for grafting-on approaches of polymer brushes using free radical polymerization [68,69] and ATRP [70,71], to mention a few examples.

While the antimicrobial properties of benzophenone-modified polysaccharides have been studied extensively, to the best of our best knowledge, there are no publications that describe benzophenone-mediated, covalent surface anchoring of chitosan to polymeric surfaces, especially PEEK, in order to exhibit its antimicrobial action on a real-world material used for medical implants and devices. In this study, we describe the successful synthesis of benzophenone-modified chitosan derivatives with varying degrees of substitution. We herein report the successful surface functionalization of PEEK with these chitosan derivatives including chemical and physical surface characterization. We also examine their antimicrobial activities, their biocompatibility according to ISO 10993–5, and their pyrogenicity as well as potentially anti-inflammatory properties.

2. Experimental

2.1. Synthesis of chitosan derivatives

Chitosan (molecular weight 100,000–300,000 g/mol, Sigma Aldrich, Germany) was dissolved in 1% (v/v) CH_3COOH in ddH_2O. A mixture of 4-benzoyl-benzoic acid in tetrahydrofuran (THF, 100 mg/mL) was added, followed by 1-ethyl-3-(3-dimethyl-aminopropyl)carbodiimide (EDC, 1 eq) was added and the mixture was then stirred at room temperature for 60 h. Derivatized chitosan was precipitated in 5-fold excess of acetone, the precipitate filtered, and re-precipitated two more times. The resulting material was dissolved in 100 mL ddH_2O and dialyzed 5 times against an excess of 1 mM hydrochloric acid. After lyophilization, the benzophenone-substituted chitosan derivatives were obtained as a white powder.

2.2. UV/vis and nuclear magnetic resonance (NMR) measurements

Benzophenone-substituted chitosan derivatives were dissolved to 5 mg/mL in 1 mM HCl. The UV/Vis absorbance (220–600 nm) of

various dilutions was measured in a Perkin Elmer Lambda XLS + photometer. Absorption at 263 nm was used to determine the degree of functionalization, which was calculated from a standard curve of 4-benzoyl-benzoic acid dissolved in ethanol, cf. Fig. S1 in Supplementary Material. Degree of substitution is given as the ratio between determined benzophenone concentration in the measured solutions and total polymer amount. NMR measurements were performed in 1 mM deuterium chloride (DCl) in D_2O in a Varian Unity 500 NMR spectrometer. Chemical shifts are reported in parts per million relative to the solvent signal (D_2O). Signals were assigned by first-order analysis.

2.3. Coating formation

To generate polyether ether ketone (PEEK) sample coatings, a rod of PEEK polymer (2 m length, 25 mm diameter, Schmidt + Bartl GmbH, Villingen-Schwenningen, Germany) was cut into 2 mm chips using a lathe; the cut edges were deburred, and a smooth surface was obtained by grinding with a lathe. The PEEK chips were washed extensively with acetone, ethyl acetate, ethanol and water in an ultrasonic bath. After drying of the chips, a 100 μL sterile-filtered solution of the benzophenone-chitosan derivatives dissolved in 1 mM HCl to a concentration of 10 mg/mL was added to cover the entire surface of the PEEK chip. The PEEK chip immersed in solution was permitted to dry overnight in a sterile cabinet to prevent dust contamination and then subjected to crosslinking with UV-light (254 nm, 3 J/cm^2) using a UV-crosslinker (AnalytikJena UVP Crosslinker 254 nm). After washing 2 times with excess 1 mM HCl and ddH_2O, the chips were vacuum-dried for 16 h and then used directly in the following experiments.

For cell culture dishes, a sterile-filtered solution of the benzophenone-chitosan derivatives in 1 mM HCl (10 mg/mL for 625 μg/cm^2, 5 mg/mL for 312 μg/cm^2, and 1 mg/mL for 62.5 μg/cm^2) was added at 20 μL per well for 96-well plates or 60 μL per well for 24-well plates. The plate was permitted to dry overnight under a sterile cabinet to prevent contamination and when then subjected to crosslinking with UV light (254 nm, 3 J/cm^2) as described above. The plates were washed two times with 1 mM HCl and once with ddH_2O (200 μL per well for 96-well plates or 1 mL per well for 24-well plates). The plates were then dried to generate the final coatings that were evaluated in cell culture and microbiology experiments.

2.4. Physicochemical surface characterization

Infrared (IR) spectra of the coated PEEK chips were obtained using a PerkinElmer Spotlight 200 FT-IR microscope that was attached to a PerkinElmer Frontier FT-IR spectrometer unit. A blank PEEK chip was used as background. Difference spectra between coated and uncoated PEEK chips were recorded to eliminate interference from PEEK signals. Microscopic images were collected using the FT-IR microscope in illumination mode and are shown without any further processing. Scanning electron microscope (SEM) images were taken at a 40° tilted angle using an XL-30 SEM (Philips, Amsterdam, Netherlands) operating at 10 kV. Samples were dried in a vacuum chamber, followed by coating with a 5 nm thick Au/Pd layer (SC7620 sputter coater, Quorum, Laughton, UK). X-ray photoelectron spectroscopy (XPS) was carried out using a Physical Instruments Quantera SXM (Physical Instruments, Chanhassen, MN, USA) equipped with a monochromatic Al K_α (1486.6 eV) X-ray source. X-ray beam had a diameter of 200 μm at 50 W, area of investigation was a square of 1.4 × 1.4 mm. SEM coupled energy dispersive X-ray spectroscopy (SEM-EDS) was carried out using a Phenom XL (Thermo Fisher Scientific, USA) equipped with BDS, SED, and EDS detectors (15 kW of acceleration voltages under high vacuum level). The sample was coated with carbon prior to analysis and a copper wire was used for electrical conduction between the sample and the manifold. The acquisition data are present in the figures acquired with the instrument. Atomic force microscope (AFM) images were recorded using a CoreAFM (Nanosurf, Liestal, Switzerland) equipped with a TAP150GD-G tip (BudgetSensors, Sofia, Bulgaria, tip radius <10 nm) in tapping mode. Coating roughness on PEEK was measured with an Alphastep 500 surface profiler (KLA Tencor) using a tip with 12.5 μm radius and a force of 61 mg. Profiles with a length of 1000 μm were obtained with a scanning speed of 50 μm/s. Coating thickness was determined by measuring the surface profile with 1000 μm length over a border of the coating to uncoated PEEK and calculated by the difference in surface levels.

2.5. Biocompatibility studies

2.5.1. Cell culture

L-929 mouse fibroblasts were obtained from Dr. Oliver Podlech (CleanControlling GmbH, Emmingen-Liptingen, Germany) and cultured in low-glucose Dulbecco's Modified Eagle Medium (DMEM), containing 10% (v/v) fetal calf serum (FCS), 1% penicillin-streptomycin (10,000 U/mL) and 1% (v/v) L-glutamine. Human umbilical vein endothelial cells (HUVECs, neonatal, pooled) were obtained from Sigma Aldrich, Germany, and cultured in endothelial cell growth medium (Sigma Aldrich, Germany). Saos-2 human osteogenic sarcoma cells (Sigma Aldrich, Germany, DSMZ No. ACC 243) were cultured in McCoy's 5a medium supplemented with 10% (v/v) FCS, 2 mM L-glutamine, and 1% penicillin-streptomycin (10,000 U/mL). Mono Mac-6 monocytes (Sigma Aldrich, Germany, DSMZ No. ACC 124) were maintained in RPMI-1640 (Sigma Aldrich, Germany) supplemented with 10% (v/v) FCS, 1 mM sodium pyruvate, 10 μg/mL human insulin (Sigma Aldrich, Germany) and 1% penicillin-streptomycin (10,000 U/mL). All cell lines used in these studies were maintained in a humidified atmosphere supplemented with 5% CO_2 at 37 °C in a tissue culture incubator (CB series C150, Binder, Tuttlingen, Germany).

2.5.2. Cytotoxicity testing: extracts

Cytotoxicity testing of polymer extracts was performed according to United States Pharmacopeia (USP) standards as previously described [36,72]. Polymer extracts were obtained by coating the wells of a 24-well plate with final polymers (Fig. 1) followed by the addition of 317 μL cell culture media identified as suitable for the cell line to be evaluated. After incubation for 24 h at 37 °C in a humidified atmosphere, 100 μL of each polymer extract was added to cells grown to adherence overnight (100,000 cells/mL). Medium supplemented with 6% (v/v) DMSO was used as a positive control. After 72 h, the medium was removed from each well and replaced with 110 μL fresh media supplemented with 10% of a 10 mM 3-(4,5-dimethylthiazol-2-yl)-2,5-diphenyltetrazolium bromide (MTT) solution in phosphate-buffered saline (PBS), followed by 4 h incubation at 37 °C and 5% CO_2 in a humidified atmosphere. in the incubator. The formed formazan crystals were solubilized with 100 μL 10% sodium dodecyl sulfate (SDS; w/v) in 10 mM HCl followed by incubation at 37 °C and 5% CO_2 in an H_2O-saturated atmosphere. Absorbance measurements (570 nm) obtained using a Tecan Infinite M200 microplate reader provide a measurement of cell viability in response to each extract; this value was calculated from the ratio/percentage of the average absorbance measured in triplicate wells of extract-treated *versus* non-treated cells. Standard deviations for each of the triplicate samples are shown as error bars.

2.5.3. Cytotoxicity testing: contact

Cytotoxicity testing based on contact with the polymer was performed as described in our previous publication [36]. A 100 μL

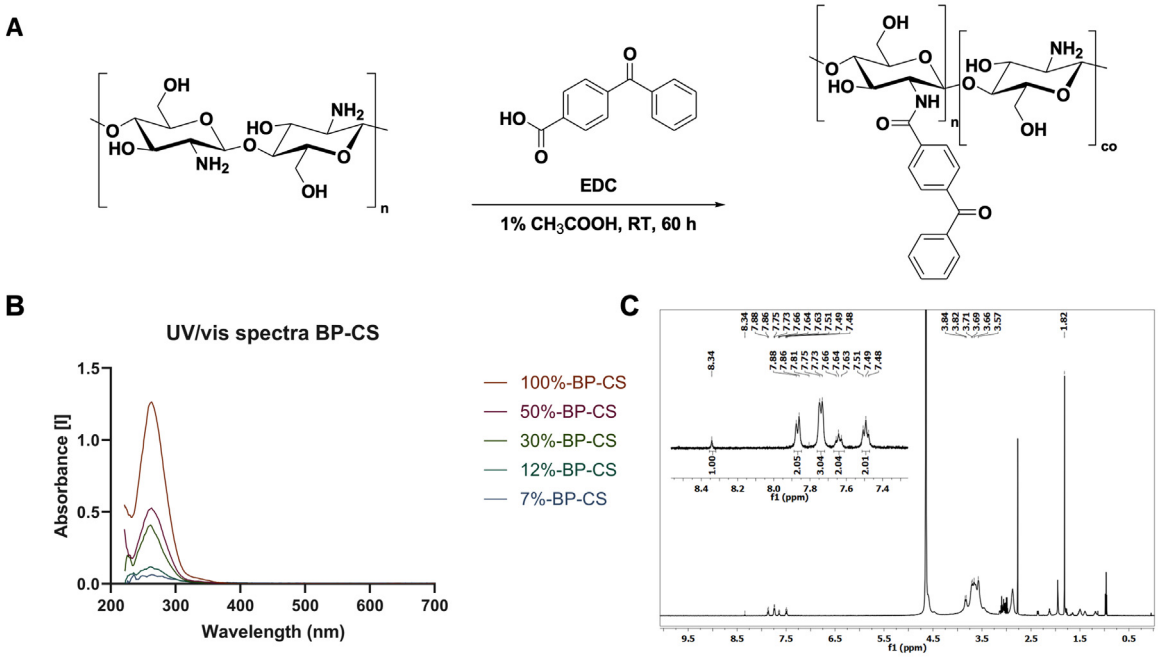

D

Polymer	EDC	4-benzylbenzoeic acid	ds calc.	ds found
100%-BP-CS	1 eq	1 eq	100%	100%
50%-BP-CS	1 eq	0.5 eq	50%	50%
30%-BP-CS	1 eq	0.25 eq	25%	30%
12%-BP-CS	1 eq	0.1 eq	10%	12%
7%-BP-CS	1 eq	0.05 eq	5%	7%

Fig. 1. Synthesis (**A**) and degree of substitution (ds) (**D**) of the chitosan derivatives. The degree of substitution determined calculated by stoichiometry matches that determined by UV/vis spectroscopy (**B**). The ^{1}H NMR spectrum confirms that the reaction between chitosan and 4-benzoyl-benzoic acid is chemoselective and results in substitution at the amino group only (**C**).

cell suspension containing 100,000 cells/mL was added to a coated 96-well plate which was then incubated for 24 or 72 h. The medium was removed from each well and replaced with 110 μL of fresh medium containing 10% of a 10 mM MTT solution in PBS. The cells were then incubated for 4 h in an incubator. This was followed by the addition of 100 μL of a 10% SDS solution in 10 mM HCl and another incubation for 4 h in an incubator. Absorbance (570 nm) was then measured using a Tecan Infinite M200 pro microplate reader. Cell viability was calculated as mean absorbance measured in wells containing polymer coatings *versus* uncoated control wells. Each measurement was performed in triplicate with error bars indicating standard deviation.

2.5.4. Interleukin (IL)-6 ELISA

Mono Mac-6 cells were used for quantitative evaluation of IL-6 expression. A 200 μL suspension containing 200,000 cells/mL was aliquoted into wells of a polymer-coated 96-well plate, followed by a 16 h incubation either with or without lipopolysaccharide (LPS, 500 ng/mL). Cells in uncoated wells treated with LPS (500 ng/mL) and untreated cells served as positive and negative controls, respectively. After 16 h incubation, the cells were collected by centrifugation (300 g, 5 min at room temperature). Levels of immunoreactive IL-6 were assessed in 100 μL samples of the resulting supernatant by ELISA according to the manufacturer's instructions (PeproTech Human IL-6 Standard ABTS ELISA Development Kit). Absorbance after reaction quenching was measured at 450 nm using a Tecan Infinite M200 microplate reader. The IL-6 concentration in each biological replicate was calculated using mean values from three triplicate wells. Error bars are used to indicate standard deviation.

2.5.5. Expression of IL-1b, IL-8, and IL-10

One million Mono Mac-6 cells in 2 mL of medium were seeded in wells of a 12-well plate coated with final benzophenone-chitosan polymers and incubated for 16 h. LPS (500 ng/mL) was used as a positive control for cytokine expression. The cells were collected by centrifugation at 350*g* for 5 min at 4 °C. The cell pellets were washed with 1 mL PBS and collected again by centrifugation. RNA was extracted from the cell pellet using the MACHEREY-NAGEL NucleoSpin® RNA Plus Kit according to the manufacturer's instructions. From the extracted RNA, 1 μg of each sample was converted into cDNA using the Thermo Scientific RevertAid First Strand cDNA Synthesis Kit according to the manufacturer's instructions. GAPDH was used as the reference gene. Quantitative gene expression analysis was performed in triplicate experiments using the Roche Light LightCycler® 480 II with Roche SYBR Green I mix according to the manufacturer's instructions. Data shown are the calculated ratios of interleukin RNA to GADPH. Error bars are used to indicate standard deviation over three triplicates.

Primer sequences include
IL-1b fwd: 5'-GAAGATGCTGGTTC-3'
IL-1b rev: 5'-TCCCATGTGTCGAAGAAGATAG-3'
IL-8 fwd: 5'-GAGCACTCCATAAGGCACAAA-3'
IL-8 rev: 5'-ATGGTTCCTTCCGGTGGT-3'
IL-10 fwd: 5'-CATAAATTAGAGGTCTCCAAAATCG-3'
IL-10 rev: 5'-AAGGGGCTGGGTCAGCTAT-3'
GAPDH fwd: 5'-CTCTGCTCCTCCTGTTCGAC-3'
GAPDH rev: 5′-CAATACGACCAAATCCGTTGAC-3'

2.6. Microbiology

2.6.1. Bacterial cell culture

Methicillin-resistant *Staphylococcus aureus* (MRSA, DSM 28766) and *Escherichia coli* (K12, DSM 498) were used in the antimicrobial assays. Glycerol stocks of these bacterial strains were stored at −80 °C. A new overnight culture was initiated for each experiment. Bacteria were incubated (Minitron, Infors HT, Bottmingen, Switzerland) at 37 °C with aeration (rotation at 100 rpm) in lysogeny broth (LB) medium. All bacterial suspensions were prepared in LB medium.

2.6.2. Antibacterial assay for the evaluation of polymer coatings

A modified version of the direct contact method based on ISO 22196 and Skytta et al. was used to evaluate the antibacterial properties of the polymer coatings [73,74]. Briefly, 200 μL of bacterial suspension a concentration of 5×10^3 cells/mL was added to each well of a coated 96-well plate. A well without polymer treatment was used for reference. The plate was sealed with parafilm to reduce evaporation and incubated for 24 h at 37 °C in a humidified incubator. The bacterial cell suspension was removed, and the wells were washed twice with 200 μL of sterile PBS. Adherent bacteria that remained in direct contact with the coating were removed with 200 μL of soybean casein digest lecithin polysorbate broth (SCDLP); the suspension was mixed thoroughly and transferred to a new 96-well plate. In addition, serial dilution of a suspension with 10^4 cells/well in SCDLP was added to the plate layout for the calculation of a calibration curve to determine the absolute reduction in bacterial count. After all empty wells were filled with sterile PBS, the plate was sealed with parafilm and placed in a Tecan Infinite M200 microplate reader that was preheated to 37 °C. Optical density at 600 nm was measured every 20 min over the next 16 h. The first derivative of the maximum rate of growth shown in each curve was calculated using GraphPad Prism 8 (San Diego, CA, USA). The live bacteria count was then determined from the calibration curve (Fig. S5) and logarithmic reductions were determined compared to results from the untreated well.

2.6.3. Bacteriostatic assay

The bacteriostatic impact of the chitosan polymers before crosslinking was evaluated according to a modified version of the assay described by Skytta et al. [73]. Briefly, 20 μL of polymer solution (concentrations including 10 mg/mL, 5 mg/mL, 1 mg/mL, 500 μg/mL, 100 μg/mL, 50 μg/mL, 10 μg/mL, 100 ng/mL, and 1 ng/mL) dissolved in 1 mM HCl, or 20 μL of 1 mM HCl as vehicle control were added to 180 μL of a bacterial suspension containing 5×10^4 cells/ml in a 96-well plate. In addition, serial dilution of 10^4 cells/well in LB media was added to the plate layout as a negative control. After all empty wells were filled with sterile PBS, the plate was sealed with parafilm and placed in a Tecan Infinite M200 microplate reader that was preheated to 37 °C. Optical density at 600 nm was measured every 20 min over the next 16 h.

The area under the growth curves between the two thresholds was calculated using GraphPad Prism 8; the lower threshold was defined as the baseline and the upper threshold was defined as the endpoint of the exponential growth phase. The areas under the growth curves for each sample were compared to those observed in suspensions exposed to vehicle control to determine relative bacterial growth. The inhibitory concentration (IC_{90}) value was calculated from these findings.

2.6.4. Crystal violet assay for biofilm assessment

Staining with crystal violet was performed to quantify biofilm formation as described previously [36]. Briefly, an overnight bacterial culture was diluted in LB medium to a concentration of 3×10^5 cells/ml. These suspensions were added to each well in a 96-well plate after the coating was washed twice with 200 μL sterile PBS. All empty wells were filled with 200 μL sterile PBS to prevent samples from drying out. The plate was then sealed with parafilm and incubated for 24 or 72 h at 37 °C in a humidified incubator without shaking. The medium was then carefully removed, and the samples were washed three times with 200 μL sterile PBS, with care taken to avoid detaching any biofilm that may have formed. This was followed by fixation with 200 μL of absolute EtOH. EtOH was then aspirated, and the samples were dried for 10 min in a sterile hood. Biofilms were then stained for 2 min in 200 μL of a 0.1% (w/v) crystal violet solution in PBS. The staining solution was removed, and samples were washed six times with 200 μL sterile PBS to remove excess dye. The samples were then dried overnight to avoid dilution errors and the dye was then released from the bacteria by adding 100 μL of absolute EtOH. The crystal violet-containing solution was transferred to a new well after 10 min incubation at room temperature and was quantified by measuring the absorbance at 595 nm in a microplate reader.

2.6.5. Live/dead staining

Live/Dead Staining was performed according to the manufacturer's instructions of the live/dead staining kit (PromoCell GmbH, Heidelberg, Germany). Briefly, polymer coatings were crosslinked in a 96-well plate and washed three times with 200 μL sterile PBS to remove residues. The sterile PBS was removed and coatings were inoculated with 200 μL of overnight bacterial culture (E.coli or MRSA) diluted to 3×10^5 cells/ml with LB medium. Samples were incubated for 24 h at 37 °C in a humidified incubator without shaking. For staining, medium was carefully removed and samples were washed three times with 200 μL sterile 150 mM NaCl solution and stained with an appropriate mixture of DMAO (ex/em 490/540) and EthD-III.

(ex/em 530/630) for 15 min at room temperature protected from light. Images were taken with the fluorescent microscope Observer. Z1 (Carl Zeiss AG, Oberkochen, Germany) and processed with ZEN blue edition (Version 3.4, Carl Zeiss AG, Oberkochen, Germany). The membrane-permeable DNA dye DMAO stains all cells (live and dead), while the membraneimpermeable DNA dye EthD-III stains only dead cells with damaged cell membranes.

3. Results and discussion

3.1. Synthesis

The reaction of chitosan with 4-benzoyl-benzoic acid in presence of EDC in the ratios shown in Fig. 1D results in the corresponding, substituted benzophenone-chitosan (BP-CS) derivatives (Fig. 1A). The degree of substitution at the chitosan glucosamine moiety was determined by UV/vis spectroscopy using a calibration curve of 4-benzoyl-benzoic acid dissolved in EtOH. The UV/vis spectrum of the benzophenone group shows a strong absorbance peak at 263 nm. The degree of chitosan substitution determined by UV/vis spectroscopy (Fig. 1B) approximately matches the values

that were calculated theoretically. Thus, the degree of chitosan functionalization could be determined stoichiometrically and is shown in Fig. 1D.

To determine whether substitution occurred at one of the hydroxyl groups or was limited to the free amino groups, we performed NMR measurements of the most highly substituted chitosan derivative (100%-BP-CS) in 1 mM DCl in D_2O (Fig. 1C). The aromatic region of the spectrum includes nine aromatic protons of the benzophenone group in two doublets (at 7.9 ppm and 7.7 ppm) and two triplets (at 7.6 ppm and 7.5 ppm). The spectrum also includes an amide signal at 8.3 ppm that is detected in an integral ratio that matches the benzophenone protons. Collectively, these results indicate that the benzophenone modification of chitosan occurs chemoselectively, as this moiety is linked to the amino but not the free hydroxyl groups. These findings confirm the structure of the benzophenone-chitosan amide derivative shown in Fig. 1A.

3.2. Surface functionalization

PEEK is a ductile polymer with mechanical properties that are similar to those of human bone [47]. This compound is not cytotoxic nor does it degrade or leach ions into the surrounding tissue [48]. Given these properties, it has been used to generate a variety of medical implants, for example, spinal cages [49-52] and endoprostheses for hip replacement [53–55]. Given its otherwise bioinert surface, multiple approaches for surface functionalization have been described, for example, deposition of inorganic substrates via atomic layer deposition (ALD) [63]. Here, the BP-CS containing solutions were solvent-cast on PEEK chips, used as a model substrate for PEEK implants, followed by UV-crosslinking at 254 nm, washing, and drying *in vacuo*. The surfaces of the solvent-cast coatings were then further investigated by XPS, SEM-EDS and IR spectroscopy.

Recorded XPS spectra of 100%-BP-CS and 30%-BP-CS coatings are shown in Fig. 2A. In general, the presence of oxygen, nitrogen and carbon could be confirmed. Al, Si, S and Cl could be detected in traces <1% (for determined atom ratios cf. Fig. S2). Due to the high presence of nitrogen in the measured coating areas, the successful coating with chitosan could be confirmed. The element ratios of carbon, nitrogen and oxygen in the 100%-BP-CS coating were also determined using SEM-EDS (cf. Fig. S3) and match the values determined via XRD within deviations of 3%, thus showing consistent data over different methods applied.

The C1s signals between 290 and 282 eV show the presence of C–C, C–H, C=C, C–O, C–N and C=O bonds. The ratio in C=O bonds, which is present in non-crosslinked benzophenone, matches the ratio 3:1 between 100%-BP-CS and 30%-BP-CS, and, therefore, is in accordance with the measurements of the degree of substitution, where 100% and 30% benzophenone content could be determined in the coatings. The relatively high difference in C–O bonds between 100%-BP-CS and 30%-BP-CS also shows successful crosslinking, since the content of C–O and C–N resulting from chitosan itself is constant, while the benzophenones carbonyl is converted into a biradicaloid triplet state, followed by hydrogen abstraction from a neighboring C–H bond and formation of a hydroxy ketyl radical, which undergoes recombination into a C–C bond while a hydroxy group is left as residue [37]. Therefore, the content of hydroxyl groups, as shown in 100%-BP-CS C1s and 30%-BP-CS C1s graphs (Fig. 2A), also differs to a certain factor, which indicates successful crosslinking of the benzophenone photophore through the C–H insertion reaction. Further, it is an additional confirmation of the degrees of substitution as determined on the chitosan polymers.

Microscopic images (200x magnification) of the coatings are shown in Fig. S4. The coarse structure of the PEEK substrate (final panel) caused by milling while cutting PEEK into slices on a lathe includes circular, groove-like structures of approximately 40 μm thickness. Coatings 100%-BP-CS, 50%-BP-CS, 12%-BP-CS, and 7%-BP-CS applied to the PEEK substrate cover these structures; by contrast, the groove-like structures remain in evidence in PEEK substrates coated with 30%-BP-CS polymer.

IR spectra of those microscopically analyzed areas are shown in Fig. 2B. The IR spectrum of the coating is generally characterized by dominant C–H bands at 2929 cm^{-1} and 2881 cm^{-1} as well as the O–H band detected at 3284 cm^{-1} which are the result of glycosidic carbon backbone C–H stretching vibrations and the free glycosidic hydroxyl groups, respectively. These measurements are consistent with literature reports of bands associated with the parent chitosan molecule [75]. Of these, the most dominant bands are those associated with the glycosidic hydroxyl groups at 3284 cm^{-1}; these are also detected in compound 30%-BP-CS, which was not visible microscopically as noted above. Collectively, these results lead us to conclude that all five coatings were formed appropriately upon UV-crosslinking of the benzophenone group with the PEEK substrate.

3.3. Surface topology

The surface topology of the coatings formed on the PEEK substrate was examined further using AFM and SEM measurements for the formed nanoscale surface topology. SEM images of the surfaces with each of the five coatings are shown in Fig. 3A. Coatings 100%-BP-CS, 50%-BP-CS, and 12%-BP-CS appear as coarse, sponge-like structures with pore diameters of ~2 μm (100%-BP-CS and 50%-BP-CS) and ~4–5 μm (12%-BP-CS). Coatings 30%-BP-CS and 7%-BP-CS appear relatively flat with lamellar-like structures. The uncoated PEEK substrate is also relatively flat; the 40 μm grooves cannot be detected at this resolution. The surface topology of the PEEK substrate measured by AFM reveals grooves of ~40 μm within the borders of resolution (Fig. 3B). The sponge-like structures associated with coatings 100%-BP-CS, 12%-BP-CS, and (to some extent) 50%-BP-CS can also be detected by this method. By contrast, coatings 30%-BP-CS and 7%-BP-CS appear as flat surfaces with underlying grooves that can be attributed to the PEEK substrate.

The surface thickness has been determined using a surface profiler, measuring over a formed edge of the polymer coating. Measured values are shown in Table 1. Overall, a surface thickness ranging between 1 and 4 μm was obtained for the coatings using the solvent casting method. The standard derivatives determined by triplicate measurements of the thickness approximately match the determined values for surface roughness, where R_a is the arithmetic average of the profile heigh deviations and R_q the quadratic average of profile heigh deviations.

Differences in the topology, resulting in either sponge-like structures or relatively flat surfaces, could be caused by differences in the degree of substitution, resulting in different solubilities in the used solvent (1 mM HCl). Chitosan itself is insoluble in water or 1 mM HCl, therefore, the reaction with 4-benzoylbenzoic acid was carried out in 1% CH_3COOH. The solubility in 1 mM HCl is, therefore, caused by the conversion of the amine into the amide functionality (cf. Fig. 1), which still leads to different solubilities through different amide-amine ratios. Solubility differences in solvent casting have been shown to influence the formation of topology using the solvent casting method and leading to inconsistencies [76]. Furthermore, the same crosslinking conditions of 3 J/cm^2 UV-light of 254 nm were applied to all coatings with different benzophenone content; we, therefore, expected differences in coating topology as shown in the SEM and AFM images. Nevertheless, the surface thickness is relatively constant in the range of 1–4 μm over all coatings as well as the determined surface roughness is.

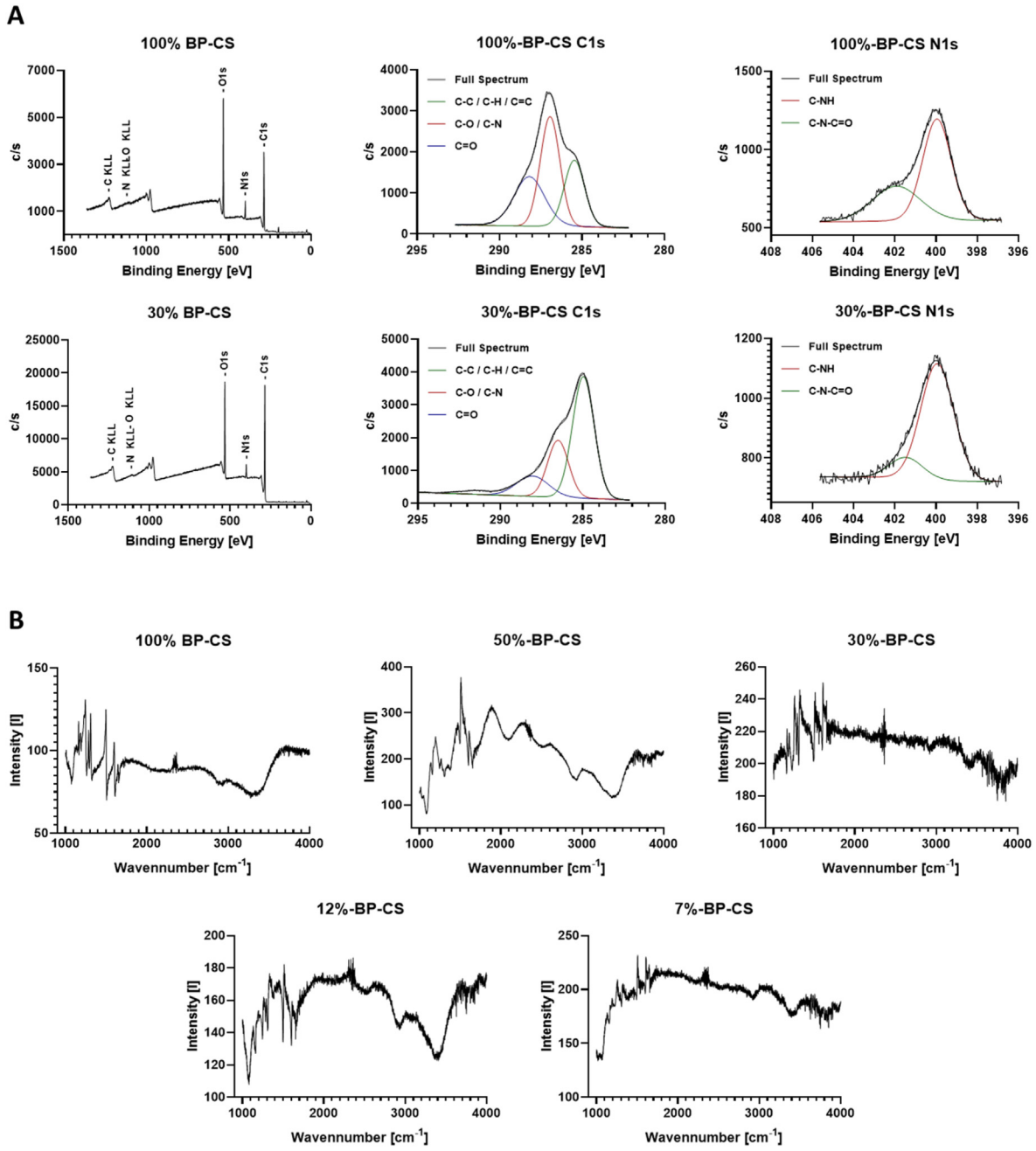

Fig. 2. XPS spectra of 100%-BP-CS and 30%-BP-CS coating on PEEK after crosslinking with UV light at 254 nm. The presence of nitrogen confirms the presence of chitosan on the coating, furthermore, the presence of C=O bonds in spectra C1s for both coatings confirm the presence of benzophenone through non-reacted residues (**A**). IR spectra of the material (**B**). The most dominant peaks in IR spectra are the glycosidic O–H bounds at 3284 cm^{-1}, followed by the glycosidic C–H stretching vibrations at both 2929 cm^{-1} and 2881 cm^{-1}. These spectra match those obtained for chitosan in this region [75] and indicate successful crosslinking of this material on the surface of the PEEK chip.

3.4. Cytotoxicity

Cytotoxicity of the synthesized coatings was determined in experiments targeting the L-929 mouse embryonal fibroblast cell line, human umbilical vein endothelial cells (HUVECs), Saos-2 osteosarcoma cell line, and Mono Mac-6 monocytes. Both extract and direct contact methods were used according to ISO 10993–5 [72,77,78]. Growth inhibition of L-929 cells in response to all extract dilutions was comparatively low (Fig. 4A). By contrast, these same dilutions (except for 30%-BP-CS) promote somewhat more substantial growth inhibition of the HUVEC cell line (Fig. 4B). Overall, little to no growth inhibition was observed in response to the 30% substituted chitosan derivative (30%-BP-CS). More substantial growth inhibition of both L-929 cells and HUVECs was observed in response to functionalized chitosan derivatives with both higher as well lower benzophenone content.

Direct contact cytotoxicity tests were performed that targeted HUVECs as well as the L929, Saos-2, and Mono Mac-6 cell lines (Fig. 4C–F). The results of these cytotoxicity tests were similar to one another. Similar to the extract tests, the 30% benzophenone-substituted chitosan derivative was minimally cytotoxic in direct contact assays targeting both HUVECs and L929 cells. Among our other results, inhibition of Saos-2 cell growth was enhanced after 72 h of contact with all chitosan derivatives evaluated; inhibition in response to compound 30%-BP-CS increased from <0% at 24 h to 40% at this time point (Fig. 4E). By contrast, the proliferation of

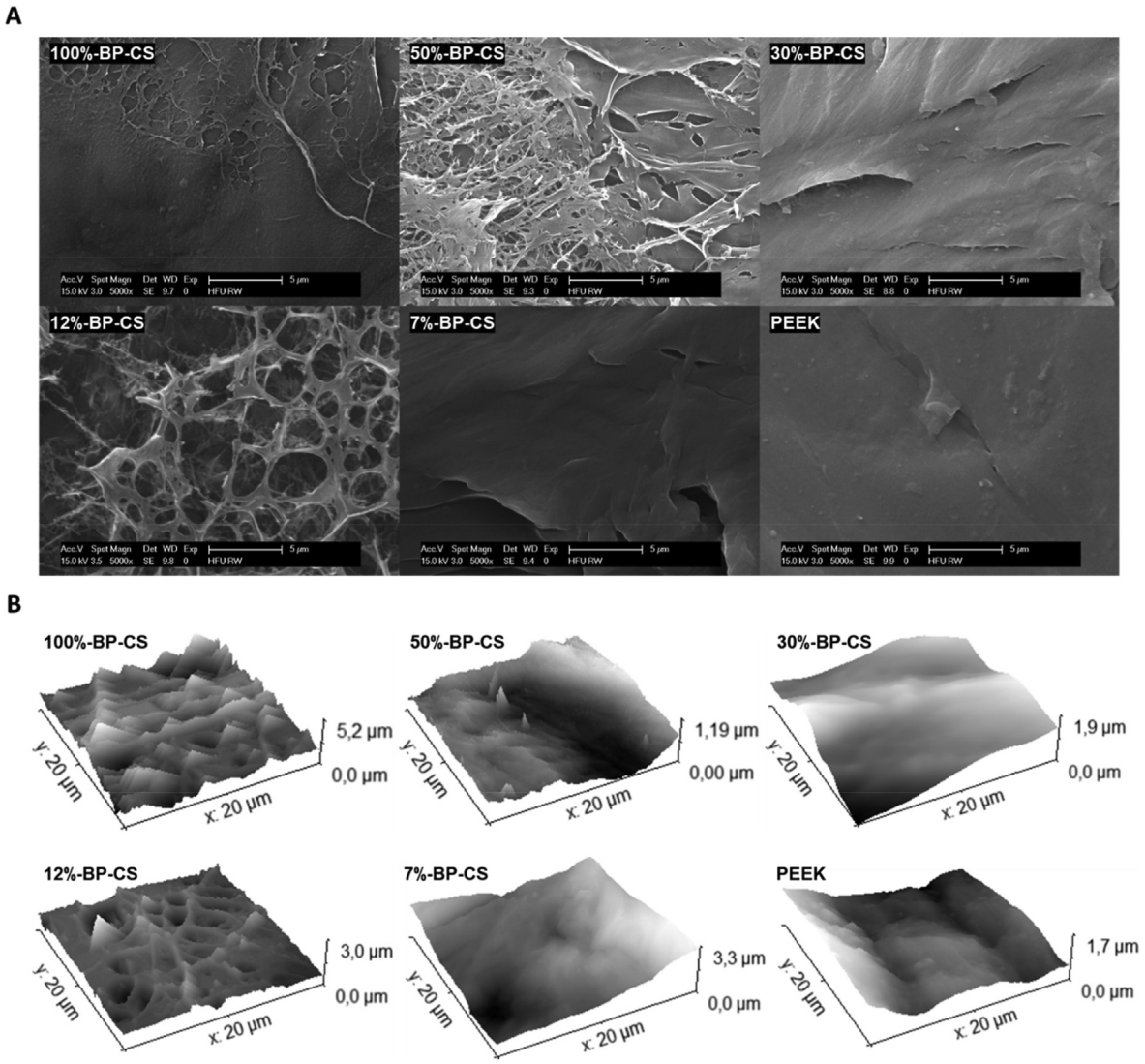

Fig. 3. SEM images (**A**) and AFM measurements (**B**) of the coatings, applied to the PEEK substrate (final panel).

Table 1
Surface thickness and surface roughness of the BP-CS coatings determined using a surface profiler.

Sample	Surface thickness [µm]	Surface roughness R_a [nm]	Surface roughness R_q [nm]
100%-BP-CS	2.15 ± 0.13	456.1	509.2
50%-BP-CS	1.46 ± 0.41	615.5	739.5
30%-BP-CS	1.51 ± 0.48	287.2	334.4
12%-BP-CS	3.75 ± 0.60	271.6	339.7
7%-BP-CS	2.12 ± 0.98	323.3	398.6

Mono Mac-6 cells remained constant, with slightly less inhibition observed in response to coatings 12%-BP-CS and 7%-BP-CS (Fig. 4F).

Benzophenone derivatives of N-acetyl glucosamine and short-chain chitooligosaccharides have been characterized as matrix metallopeptidase (MMP) inhibitors with potent activity against cancer cells [79] with potential utility as adjuvant anti-cancer therapy [80]. The activity of these compounds against sarcoma-type cells may explain some of the growth inhibition and decreased cell viability observed in cytotoxicity assays performed in this study. The doubling time of the Saos-2 sarcoma cell line is 40 h [81]. Thus, the growth inhibition of this cell type is observed most prominently at the 72 h time point, most notably in experiments performed with coating 30%-BP-CS. Downregulation of MMP2 and MMP-9 has also been linked to diminished angiogenesis and reduced migration of human endothelial cells [82]; these findings may explain the decreased viability observed in HUVEC cultures at 24 and 72 h. Results from previous studies suggest that chitosan may form polyelectrolyte complexes in culture medium that sequester growth factors provided by FCS and that this will ultimately result in decreased fibroblast proliferation. In literature, this effect was not observed in cell cultures that were not supplemented with FCS [83]. In the current study, exposure to the 30% substituted chitosan derivative 30%-BP-CS results in the retention of ~70% of the original proliferative activity relative to untreated cells at both 24 and 72 h in all cell lines evaluated. Thus, derivative 30%-BP-CS has been identified as non-cytotoxic. Interestingly, the 30%-BP-CS chitosan derivative is also most effective at inhibiting the growth and viability of both *E. Coli* and *S. aureus* bacterial strains.

3.5. Anti-inflammatory potential

The pyrogenicity of the coating surface and/or the presence of potential pyrogenic residues or contaminants was elucidated by a

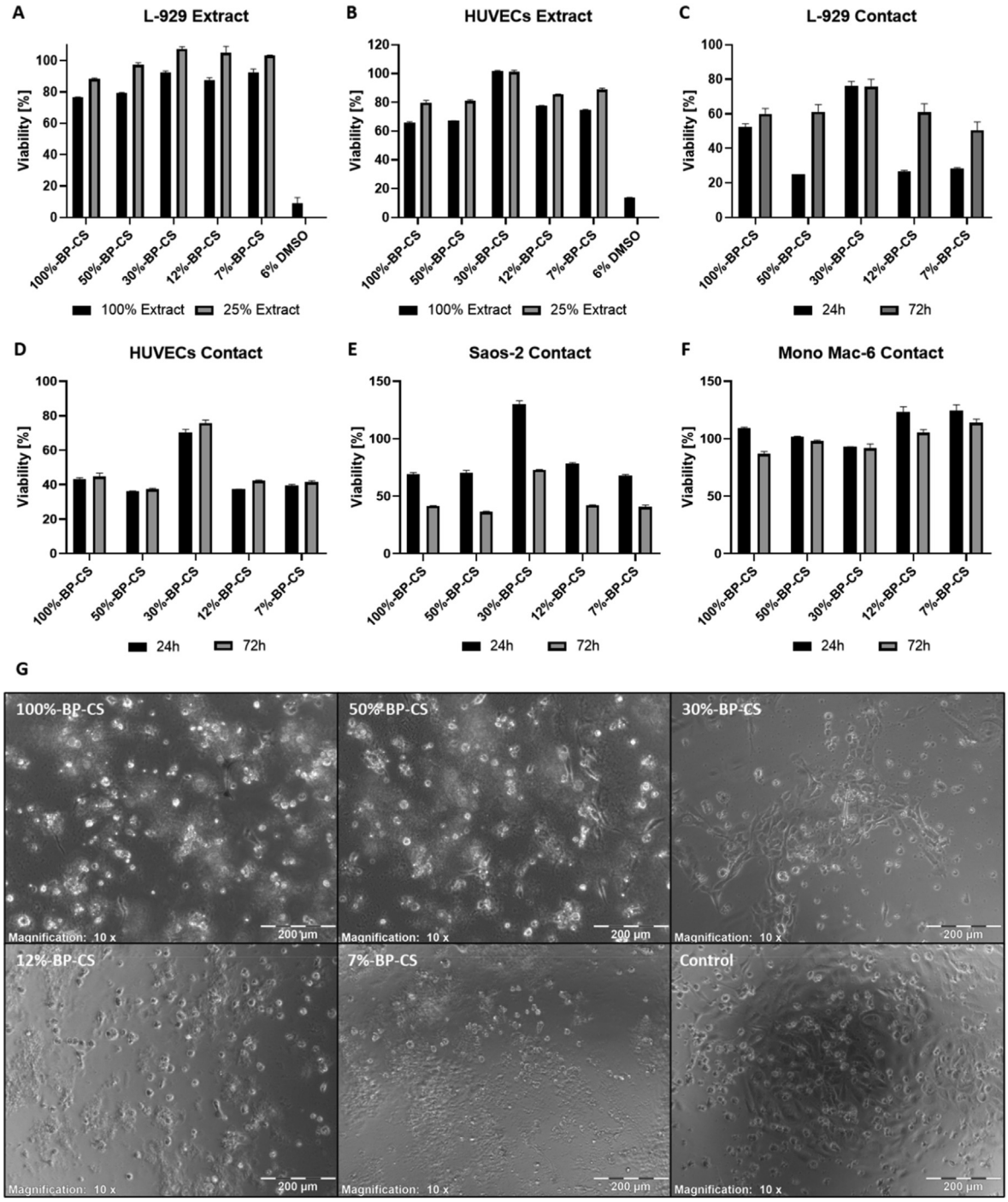

Fig. 4. Cytotoxicity at 24 and 72 h associated with exposure to extracts of BP-CS coatings in L-929 cells and HUVECs with 6% DMSO as positive control (**A**, **B**). Cytotoxicity at 24 and 72 h associated with direct contact of L-929, HUVECs, Saos-2, and Mono Mac-6 with BP-CS coatings (**C**–**F**). Error bars are given as standard derivation of triplicates each. In (**G**) L-929 mouse fibroblasts growing on the coated surface at 72 h before the addition of the MTT reagent. Cytotoxicity is observed in response to contact with polymers 100%-BP-CS, 50%-BP-CS, 12%-BP-CS, and 7%-BP-CS. By contrast, relatively little cytotoxicity is observed in response to contact with polymer 30%-BP-CS. This result was confirmed by the cell viability test evaluated quantitatively in (**C**); the images shown are at 10x magnification.

monocyte activation test using the Mono Mac-6 cell line and an enzyme-linked immunosorbent assay (ELISA) for quantitative detection of IL-6 secretion [84,85]. An approximately two-fold increase in IL-6 was detected in the medium of cultures grown in wells with 625 μg/cm^2 of 100%-BPCS, 50%-BP-CS, 12%-BP-CS and 7%-BP-CS coatings compared to negative controls (Fig. 5A, left). By contrast, no increase in IL-6 levels was detected in wells coated with 30%-BP-CS derivative. No significant increases in IL-6 release were observed over control levels in cultures grown in wells coated with lower concentrations of these chitosan derivatives. Thus, all coatings can be considered non-pyrogenic when used at concentrations at or below 312.5 μg/cm^2; 30%-BP-CS derivative is non-pyrogenic at concentrations as high as 625 μg/cm^2. We also evaluated the expression of genes encoding the cytokines IL-1b, IL-8, and IL-10 in monocytes that were cultivated for 16 h in coated wells. We detected no significant increase in IL-1b expression in

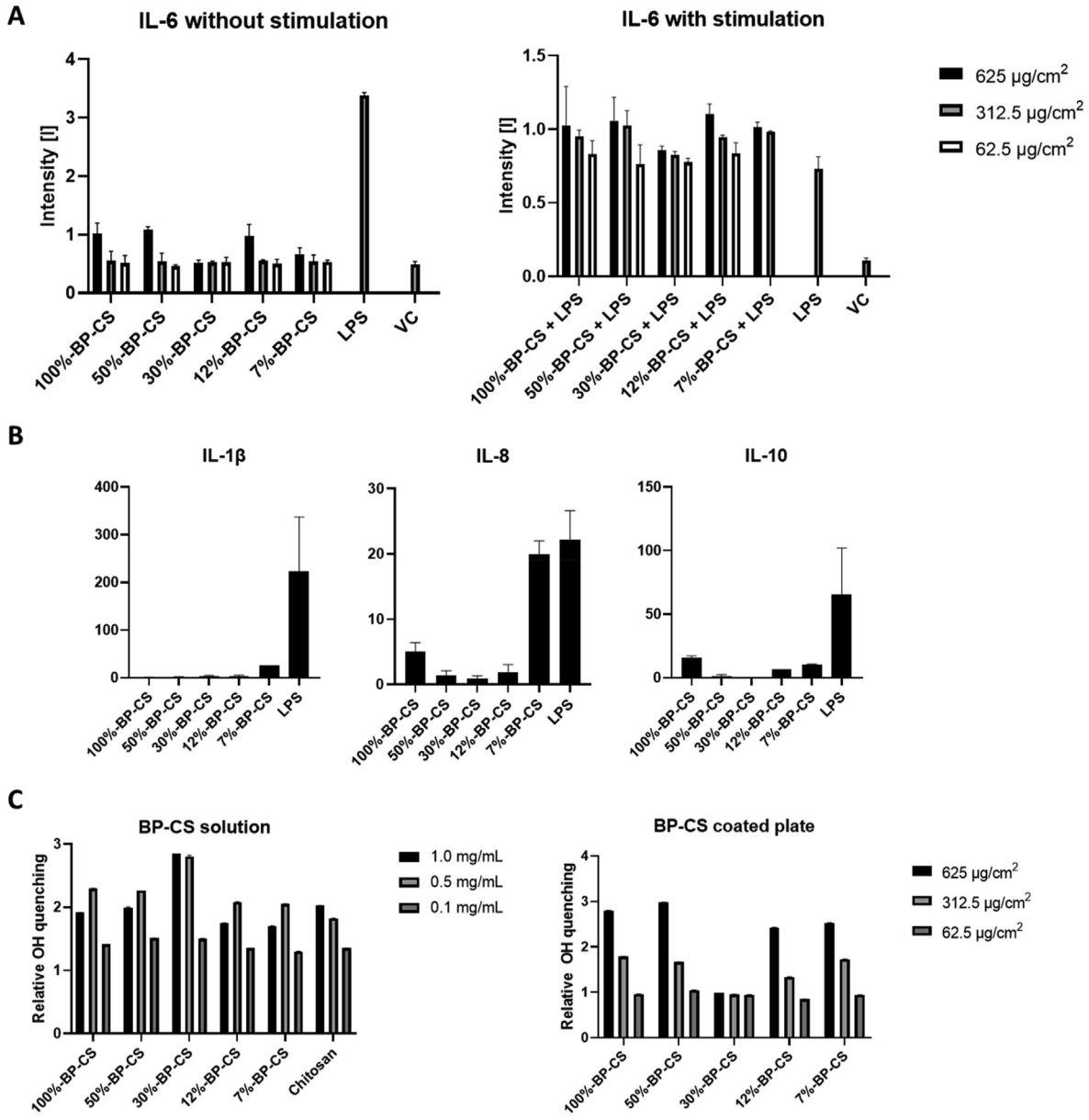

Fig. 5. Secreted IL-6 from Mono Mac-6 monocytes (**A**) detected in the medium by ELISA at 16 h both with (left) and without (right) stimulation with 500 ng/mL LPS together with LPS and vehicle control (VC) alone. IL-6 levels are twice as high in LPS-stimulated monocytes exposed to 625 µg/cm^2 coatings compared to vehicle control (VC). By contrast, IL-6 levels remain at baseline in cell cultures exposed to lower coating concentrations. IL-6 levels remained at baseline in all cultures exposed to coating 30%-BP-CS. Expression of IL-1b, IL-8, and IL-10 genes (**B**) determined by qPCR after 16 h cultivation on a benzophenone-substituted chitosan-coated microtiter plate (625 µg/cm^2). Expression of all three cytokine genes remained at or near baseline in cultures exposed to polymer 30%-BP-CS. (**C**) Radical (OH·) quenching mediated by benzophenone-substituted chitosan polymers in solution compared to unmodified chitosan (left) and as coatings on microtiter plates.

Mono Mac 6 cells cultured with derivatives 100%-, 50%-, 30%- and 12%-BP-CS, compared to the LPS-positive control [63]. A similar pattern was observed for IL-8; this might be related to findings indicating that IL-8 expression is induced by exogenous IL-1b in monocytes [86]. The lowest level of IL-8 expression was detected in cells cultured with 30%-BP-CS derivative; expression levels increase from 50%_BP-CS to 100%-BP-CS and from 12%-BP-CS, reaching a maximum in the presence of 7%-BP-CS, approaching the levels observed in response to the LPS positive control. Expression of the anti-inflammatory cytokine, IL-10 increases in a similar pattern, which may represent its capacity to modulate the responses of the proinflammatory cytokines IL-1b, IL-6, and IL-8. Interestingly, the expression of IL-10 is more prominent in response to 100%-BP-CS derivative than 7%-BP-CS; the 100%-BP-CS derivative also elicits comparatively lower levels of both IL-6 and IL-8. Overall, we can conclude that the 30%-BP-CS coating is non-inflammatory, while the 100%-BP-CS coating exhibits anti-inflammatory properties as described above.

LPS induces oxidative stress via the production of reactive oxygen species (ROS) in both monocytes and macrophages. LPS-mediated monocyte activation also leads to the synthesis and release of proinflammatory cytokines, including IL-1b, followed by IL-6 and IL-8, which are cytokines that stimulate local inflammation [87-89]. Chitosan has characterized antioxidative properties and is capable of quenching hydroxyl- and superoxide radicals in solution [90]. Chitosan also exhibits anti-inflammatory properties including its capacity to limit the expression of cyclooxygenase (COX)-2 [91–93]. We tested the radical scavenging potential of each coating and examined their capacity to suppress monocyte-mediated IL-6 release in response to 500 ng/mL LPS. ROS is generated in biological

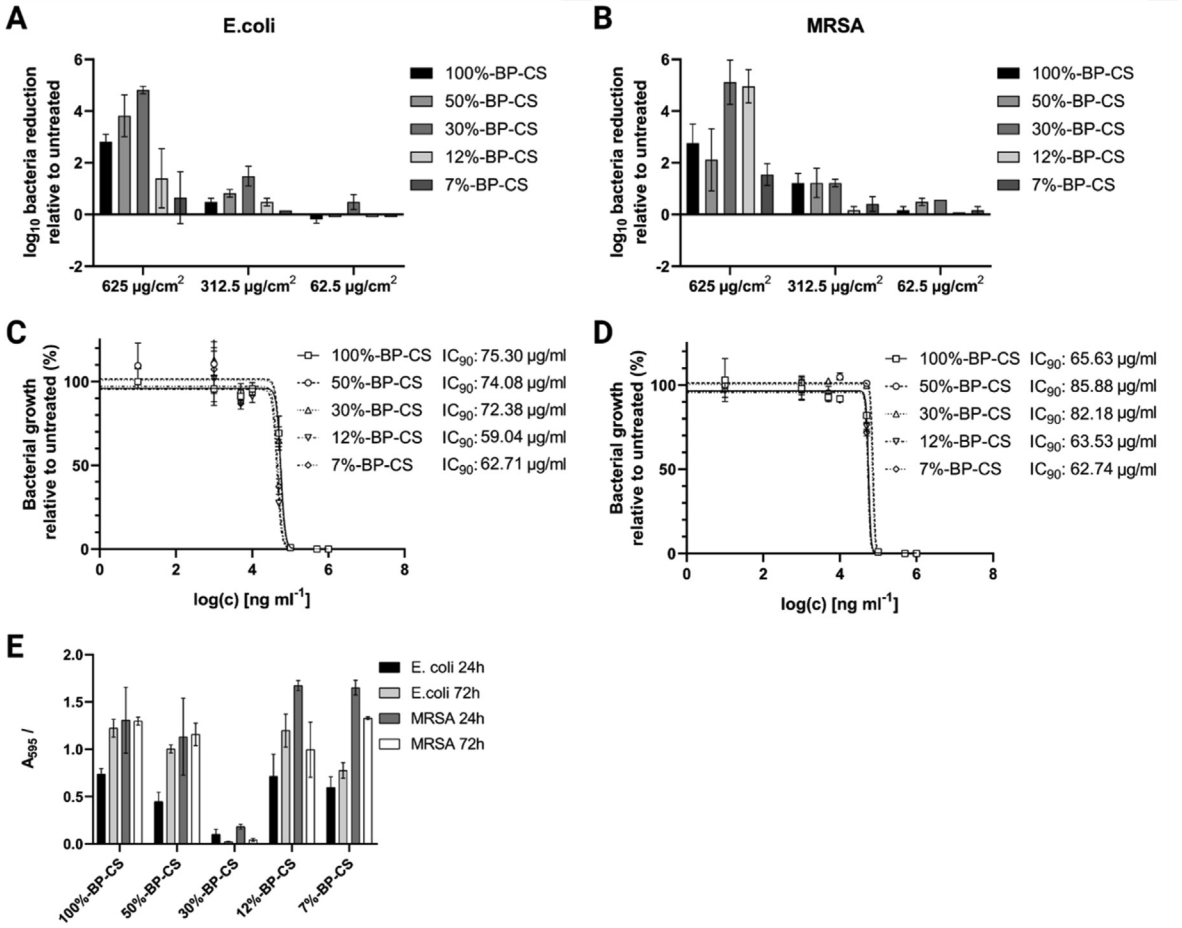

Fig. 6. Antimicrobial activity of benzophenone-substituted chitosan coatings and solubilized chitosan derivatives. Shown are reductions in the number of viable *E. coli* (**A**) and MRSA (**B**) that are adherent to coatings relative to the untreated surface of a tissue culture plate. The impact of solubilized chitosan derivatives at various concentrations on the growth of *E. coli* (**C**) and MRSA (**D**) and the calculated IC_{90} values. (**E**) Biofilms of *E. coli* and MRSA at 24 and 72 h were evaluated by crystal violet staining. All values represent means ± standard deviations; n = 3.

systems mainly via the Fenton reaction [94]. Thus, we performed this reaction in an *ex vivo* as described by Li et al. [90] that utilized photometric measurements of Safranin O degradation mediated by hydroxyl radicals [90]. We found that compound 30%-BP-CS was most effective at radical quenching; exposure to polymers of this compound in solution resulted in a 3-fold increase in OH-quenching compared to the negative control (Fig. 5C). Interestingly, the effectiveness of coating 30%-BP-CS exceeds that of chitosan alone by a factor of 1.5, also compared to the negative control. However, these anti-oxidant activities were not detected when compound 30%-BP-CS was evaluated as a coating. Furthermore, and despite their capacity for radical quenching, none of the coatings had an impact on monocytes-mediated IL-6 secretion compared to the responses of unstimulated monocytes alone (see Fig. 5A, right).

In conclusion, we found that exposure to coating 30%-BP-CS resulted in no increase in proinflammatory cytokine release; this coating also had a negligible effect on modulating the responses of LPS-stimulated monocytes. Monocyte viability remained at or near 100% after 24 or 72 h in a contact with this coating. Based on these results, we identify coating 30%-BP-CS as both inert and biocompatible in experiments performed in relevant *ex vivo* settings.

3.6. Antimicrobial properties

The antibacterial properties of soluble chitosan are well-characterized. Among these findings, Li et al. [95] reported that chitosan at ~0.1% (w/v) resulted in >80% inhibition of several bacterial strains. In this study, we tested our compounds within a general range of concentrations to determine the 90% inhibitory concentration (IC_{90}) based on the results of growth curves of *E. coli* and MRSA (Fig. S3). Our findings revealed that all five BP-CS derivatives retained their antibacterial properties when evaluated in solution (Fig. 6C and D). The IC_{90}s determined for benzophenone chitosan derivatives targeting *E. coli* were 75, 74, 72, 59, and 63 µg/mL, respectively; IC_{90}s determined for chitosan derivatives targeting MRSA were 66, 86, 82, 64, and 63 µg/mL, respectively. These calculated IC_{90} values are comparable to the minimum inhibitory concentrations previously reported for non-functionalized chitosan against *E. coli* (50 µg/mL) and MRSA (100 µg/mL) [96]. Interestingly, although benzophenone is considered toxic to bacteria [97], higher IC_{90} values were observed for compounds with higher benzophenone content. The reduced impact associated with more extensive substitution may be explained by reductions in the number of free amino groups contributing to the overall cationic charge of the polymer. Of note, according to the SMH model, cationic charge is the critical feature underlying chitosan-mediated antimicrobial activity [5,6]. Thus, our results suggest that the impact of the loss of cationic charge may exceed the potential for increased toxicity associated with an increase in the benzophenone content. This net effect may result in an overall reduction of its antibacterial properties.

We then examined the antibacterial properties of coatings prepared from the dissolved chitosan derivatives after UV-

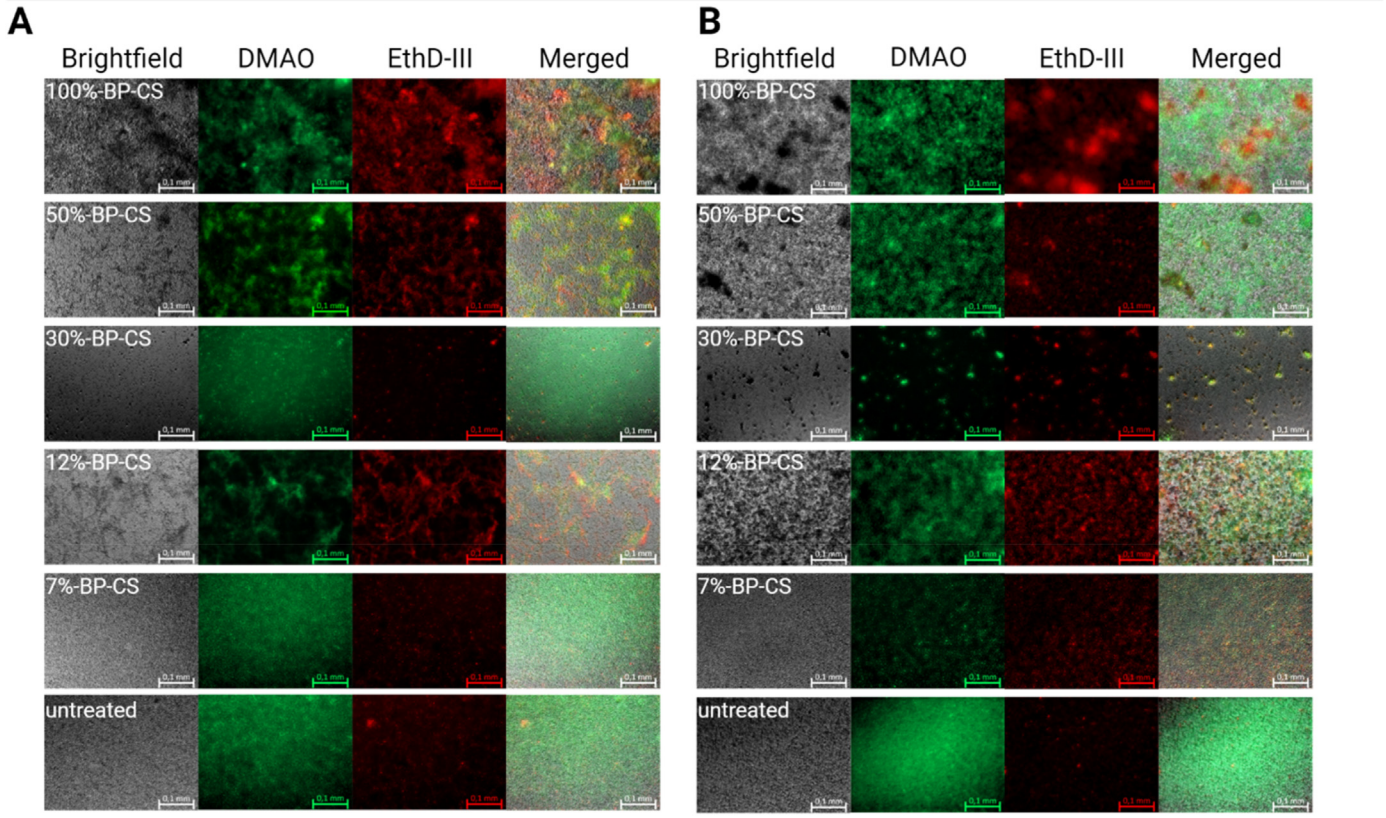

Fig. 7. Representative microscopic images of Live/Dead stained E. coli (**A**) and MRSA (**B**) after 24 h incubation on the corresponding polymer-coated or untreated surface of a 96-well cell culture plate. Magnification is 200x; scale bar measures 0.1 mm.

crosslinking. Polymer coatings were prepared at mass-to-surface ratios of 625, 312.5, and 62.5 μg/cm^2. Our results revealed a net reduction in antibacterial efficacy of all coatings that paralleled the decreases in mass-to-surface ratios (Figs. S2, 6A, and 6B).

Maximum antibacterial activity was observed for coating of 30%-BP-CS applied at 625 μg/cm^2. Direct contact with this coating (30% benzophenone) resulted in an approximately 5-log reduction of viable *E. coli* or MRSA. Compounds with higher (100%-BP-CS and 50%-BP-CS) and lower (12%-BP-CS and 7%-BP-CS) benzophenone contents were not as effective at limiting bacterial viability (Fig. 6A and B). These results indicate that the antibacterial activity of the cross-linked compound in the form of a coating may be more effective than the individual components in solution. In the case of benzophenone derivatives, crosslinking is critical to ensure a uniform and functional coating.

We also examined biofilm formation on the polymer coatings at 24 and 72 h by crystal violet (CV) staining (Fig. 6E) and Live/Dead staining (Fig. 7). These observations confirmed the results of previous experiments as they revealed that coating 30%-BP-CS was more effective than the other four benzophenone-substituted coatings evaluated. Coating 30%-BP-CS was the only derivative that promoted a reduction in the level of CV stained *E. coli* biofilm between the 24 and 72 h time points, to a point at which it was nearly undetectable. Similar results were obtained in experiments targeting MRSA. However, it is also worth noting that no increases in biofilm formation were observed by CV staining between 24 and 72 h for MRSA in experiments performed with the four additional coatings; experiments performed with coatings 12%-BP-CS and 7%-BP-CS revealed reductions in the amounts of CV stained MRSA biofilms during this time interval. Live/dead staining confirmed that, after 24 h, there was considerably less biofilm on coating 3c and almost all cells still present were stained as dead. In contrast, the other coatings had developed biofilms, albeit with a higher percentage of dead cells compared to the untreated control. Collectively, the results suggest that these compounds are more effective against biofilms generated by Gram-positive bacteria such as MRSA compared to Gram-negative bacteria, such as *E. coli*.

4. Conclusion

In this study, our findings document the successful functionalization of the free amino groups of chitosan with benzophenone moieties. The degree of functionalization obtained approximately matched the stoichiometrically-calculated ratios. Chemoselective functionalization of the free amino groups via amide formation was confirmed by NMR spectroscopy. Coatings prepared from 30% functionalized derivative, named 30%-BP-CS, were the most effective of the group against the bacterial pathogens MRSA and *E. coli*, which were used as clinically relevant microbial strains in antimicrobial testing. The 30%-BP-CS derivative also exhibited the least cytotoxicity when evaluated in cultures of L-929 fibroblasts, HUVECs, Saos-2 osteoblasts, and Mono Mac-6 monocytes using ISO 10993−5 testing methodology for cytotoxicity assessment. No inflammation was observed in response to the 30%-BP-CS coating in the pyrogen test performed as per ISO 10993−11. Thus, the 30%-BP-CS coating can be considered biologically inert. Interestingly, this 30% functionalized chitosan shows the optimum properties with respect to antimicrobial action and biocompatibility under the UV-crosslinking conditions applied. Different levels of benzophenone substitution (both higher and lower) lead to reduced biocompatibility, a greater potential for inflammation, and diminished antimicrobial activity. This may relate at least in part to differences in

crosslinking efficiency under the applied conditions (3 J/cm^2, 254 nm), leading to different amounts of uncrosslinked benzophenone residues, which have been shown in the XPS spectra (Fig. 2A). The appropriate combination of these factors may lead to the thinnest possible coating and a smoother surface by minimizing pore formation and the concentration of benzophenone residues that remain uncrosslinked. Previous studies have suggested that the smoothness of the surface is a critical determinant of the biocompatibility and inflammatory potential of biomedical implants [98]. The XPS and IR spectra (Fig. 2) and AFM and SEM measurements (Fig. 3) support this conclusion; these studies revealed that the 30%-BP-CS coating exhibited a relatively smooth surface with no visible pores or sponge-like structures that may promote cell adhesion and inflammation. However, the surface roughness of the 30%-BP-CS coating is slightly higher than the roughness of the 12%-BP-CS coating. This property might also explain the limited capacity for OH-radical quenching (Fig. 4); coatings prepared from 30%-BP-CS derivative display comparatively less active surface area for radical quenching. This can explain the relatively bioinert properties of this coating despite the fact that IC_{90} of the polymers were within range of those exhibited by the other compounds when they were all examined in solution. However, when applied as a coating, their capacity for growth inhibition differed significantly (Fig. 5). While the exactly optimized parameters for crosslinking conditions and surface properties of the coatings still need more adjustment, overall, our study presents an interesting chemical approach that can be used to generate chitosan-derived coatings for implant materials that are biocompatible, non-inflammatory, and antimicrobial with potential for use in photopatterning applications.

Credit author statement

Max Borgolte: Conceptualization, Methodology, Investigation, Writing – Original Draft, Writing – Review & Editing, Visualization. Oliver Riester: Methodology, Investigation, Writing – Original Draft, Writing – Review & Editing, Visualization. **Isabel Quint**: Investigation, Writing – Review & Editing. Felix Blendinger: Investigation, Visualization, Writing – Review & Editing. **Volker Bucher**: Resources, Writing – Review & Editing. Stefan Laufer: Resources, Writing – Review & Editing. René Csuk: Resources, Writing – Review & Editing. Luca Scotti: Investigation, Visualization, Resources. Hans-Peter Deigner: Conceptualization, Writing – Review & Editing, Project administration, Funding acquisition, Resources.

Funding

Funding was granted by CoHMed FunctioMed (FKz: 13FH5I02IA), CoHMed MS-ToxTest (FKz 13FH5E01IA) and CoHMed PersonaMed (FKz: 13FH5I06IA), all BMBF, as well as TriMaBone–Trinationale Forschungsinitiative: 3D-Druck Materialien für resorbierbare Knochen-implantate" (Europäischer Fonds für regionale Entwicklung—EFRE) in the program "Interreg VOberrhein" (Ref: 5115/3.17).

Declaration of competing interest

The authors declare that they have no known competing financial interests or personal relationships that could have appeared to influence the work reported in this paper.

Data availability

No data was used for the research described in the article.

Acknowledgments

We thank Dr. Oliver Podlech, CleanControlling GmbH, for providing us with the L-929 cell line used for biocompatibility testing as well as technical support regarding cell handling and ISO 10993-5 biocompatibility testing. We also thank Dr. Dagmar Martin and Duva Giuliano from the Natural and Medical Sciences Institute (NMI) at the University of Tubingen, Germany, for performing the XPS measurements and gratefully acknowledge their support regarding analysis and discussion of the obtained data. Continuous stimulation by N.C.R. is gratefully acknowledged.

Appendix A. Supplementary data

Supplementary data to this article can be found online at https://doi.org/10.1016/j.mtchem.2022.101176.

References

[1] I.M. Helander, E.L. Nurmiaho-Lassila, R. Ahvenainen, J. Rhoades, S. Roller, Chitosan disrupts the barrier properties of the outer membrane of Gram-negative bacteria, Int. J. Food Microbiol. 71 (2001) 235–244, https://doi.org/10.1016/S0168-1605(01)00609-2.
[2] J.Y. Je, S.K. Kim, Chitosan derivatives killed bacteria by disrupting the outer and inner membrane, J. Agric. Food Chem. 54 (2006) 6629–6633, https://doi.org/10.1021/jf061310p.
[3] K. Divya, S. Vijayan, T.K. George, M.S. Jisha, Antimicrobial properties of chitosan nanoparticles: mode of action and factors affecting activity, Fibers Polym. 18 (2017) 221–230, https://doi.org/10.1007/s12221-017-6690-1.
[4] R.C. Chien, M.T. Yen, J.L. Mau, Antimicrobial and antitumor activities of chitosan from shiitake stipes, compared to commercial chitosan from crab shells, Carbohydr. Polym. 138 (2016) 259–264, https://doi.org/10.1016/J.CARBPOL.2015.11.061.
[5] Y. Shai, Mechanism of the binding, insertion and destabilization of phospholipid bilayer membranes by α-helical antimicrobial and cell non-selective membrane-lytic peptides, Biochim. Biophys. Acta Biomembr. 1462 (1999) 55–70, https://doi.org/10.1016/S0005-2736(99)00200-X.
[6] K. Matsuzaki, Why and how are peptide–lipid interactions utilized for self-defense? Magainin and tachyplesins as archetypes, Biochim. Biophys. Acta, Biomembr. 1462 (1999) 1–10, https://doi.org/10.1016/S0005-2736(99)00197-2.
[7] X. Li, X. Feng, S. Yang, G. Fu, T. Wang, Z. Su, Chitosan kills Escherichia coli through damage to be of cell membrane mechanism, Carbohydr. Polym. 79 (2010) 493–499, https://doi.org/10.1016/j.carbpol.2009.07.011.
[8] R.P. Carlson, R. Taffs, W.M. Davison, P.S. Stewart, Anti-biofilm properties of chitosan-coated surfaces, J. Biomater. Sci. Polym. Ed. 19 (2008) 1035–1046, https://doi.org/10.1163/156856208784909372.
[9] X. Fei Liu, Y. Lin Guan, D. Zhi Yang, K. de Yao, Antibacterial Action of Chitosan and Carboxymethylated Chitosan, 2000, https://doi.org/10.1002/1097-4628.
[10] A.J. Varma, S.V. Deshpande, J.F. Kennedy, Metal complexation by chitosan and its derivatives: a review, Carbohydr. Polym. 55 (2004) 77–93, https://doi.org/10.1016/j.carbpol.2003.08.005.
[11] P. Sahariah, M. Másson, Antimicrobial chitosan and chitosan derivatives: a review of the structure–activity relationship, Biomacromolecules 18 (2017) 3846–3868, https://doi.org/10.1021/ACS.BIOMAC.7B01058.
[12] Y.C. Chung, H.L. Wang, Y.M. Chen, S.L. Li, Effect of abiotic factors on the antibacterial activity of chitosan against waterborne pathogens, Bioresour. Technol. 88 (2003) 179–184, https://doi.org/10.1016/S0960-8524(03)00002-6.
[13] H. Liu, Y. Du, J. Yang, H. Zhu, Structural characterization and antimicrobial activity of chitosan/betaine derivative complex, Carbohydr. Polym. 55 (2004) 291–297, https://doi.org/10.1016/J.CARBPOL.2003.10.001.
[14] H. Liu, Y. Du, X. Wang, L. Sun, Chitosan kills bacteria through cell membrane damage, Int. J. Food Microbiol. 95 (2004) 147–155, https://doi.org/10.1016/j.ijfoodmicro.2004.01.022.
[15] W. Samprasit, R. Kaomongkolgit, M. Sukma, T. Rojanarata, T. Ngawhirunpat, P. Opanasopit, Mucoadhesive electrospun chitosan-based nanofibre mats for dental caries prevention, Carbohydr. Polym. 117 (2015) 933–940, https://doi.org/10.1016/J.CARBPOL.2014.10.026.
[16] E.A. Izano, I. Sadovskaya, E. Vinogradov, M.H. Mulks, K. Velliyagounder, C. Ragunath, W.B. Kher, N. Ramasubbu, S. Jabbouri, M.B. Perry, J.B. Kaplan, Poly-N-acetylglucosamine mediates biofilm formation and antibiotic resistance in Actinobacillus pleuropneumoniae, Microb. Pathog. 43 (2007) 1–9, https://doi.org/10.1016/j.micpath.2007.02.004.
[17] Y. Zheng, N. Pan, Y. Liu, X. Ren, Novel porous chitosan/N-halamine structure with efficient antibacterial and hemostatic properties, Carbohydr. Polym. 253 (2021), 117205, https://doi.org/10.1016/J.CARBPOL.2020.117205.

[18] G.M. Luz, L. Boesel, A. Del Campo, J.F. Mano, Micropatterning of bioactive glass nanoparticles on chitosan membranes for spatial controlled biomineralization, Langmuir 28 (2012) 6970–6977, https://doi.org/10.1021/la300667g.
[19] Y. Wang, R. Shi, P. Gong, J. Li, J. Li, D. Ao, P. Wang, Y. Yang, Y. Man, Y. Qu, Bioelectric effect of a chitosan bioelectret membrane on bone regeneration in rabbit cranial defects, J. Bioact. Compat Polym. 27 (2012) 122–132, https://doi.org/10.1177/0883911512436773.
[20] I.-Y. Kim, S.-J. Seo, H.-S. Moon, M.-K. Yoo, I.-Y. Park, B.-C. Kim, C.-S. Cho, Chitosan and its derivatives for tissue engineering applications, Biotechnol. Adv. 26 (2008) 1–21, https://doi.org/10.1016/j.biotechadv.2007.07.009.
[21] P.R. Sivashankari, M. Prabaharan, Prospects of chitosan-based scaffolds for growth factor release in tissue engineering, Int. J. Biol. Macromol. 93 (2016) 1382–1389, https://doi.org/10.1016/j.ijbiomac.2016.02.043.
[22] Z. Liu, H. Wang, Y. Wang, Q. Lin, A. Yao, F. Cao, D. Li, J. Zhou, C. Duan, Z. Du, Y. Wang, C. Wang, The influence of chitosan hydrogel on stem cell engraftment, survival and homing in the ischemic myocardial microenvironment, Biomaterials 33 (2012) 3093–3106, https://doi.org/10.1016/j.biomaterials.2011.12.044.
[23] W. Shi, D. Nie, G. Jin, W. Chen, L. Xia, X. Wu, X. Su, X. Xu, L. Ni, X. Zhang, X. Zhang, J. Chen, BDNF blended chitosan scaffolds for human umbilical cord MSC transplants in traumatic brain injury therapy, Biomaterials 33 (2012) 3119–3126, https://doi.org/10.1016/j.biomaterials.2012.01.009.
[24] R. Jayakumar, M. Prabaharan, P.T. Sudheesh Kumar, S.V. Nair, H. Tamura, Biomaterials based on chitin and chitosan in wound dressing applications, Biotechnol. Adv. 29 (2011) 322–337, https://doi.org/10.1016/j.biotechadv.2011.01.005.
[25] R. Jayakumar, M. Prabaharan, S.V. Nair, S. Tokura, H. Tamura, N. Selvamurugan, Novel carboxymethyl derivatives of chitin and chitosan materials and their biomedical applications, Prog. Mater. Sci. 55 (2010) 675–709, https://doi.org/10.1016/j.pmatsci.2010.03.001.
[26] B. Pidhatika, N. Zhao, M. Zinggeler, J. Rühe, Surface-attached dual-functional hydrogel for controlled cell adhesion based on poly(N,N-dimethylacrylamide), J. Polym. Res. 26 (2019) 1–12, https://doi.org/10.1007/s10965-019-1728-2.
[27] P. Samyn, M. Biesalski, O. Prucker, J. Rühe, Confining acrylate-benzophenone copolymers into adhesive micropads by photochemical crosslinking, J. Photochem. Photobiol. Chem. 377 (2019) 80–91, https://doi.org/10.1016/j.jphotochem.2019.03.040.
[28] F.D. Scherag, R. Niestroj-Pahl, S. Krusekopf, K. Lücke, T. Brandstetter, J. Rühe, Highly selective capture surfaces on medical wires for fishing tumor cells in whole blood, Anal. Chem. 89 (2017) 1846–1854, https://doi.org/10.1021/acs.analchem.6b04219.
[29] F.D. Scherag, A. Mader, M. Zinggeler, N. Birsner, R.E. Kneusel, T. Brandstetter, J. Rühe, Blocking-free and substrate-independent serological microarray immunoassays, Biomacromolecules 19 (2018) 4641–4649, https://doi.org/10.1021/acs.biomac.8b01334.
[30] L. Yuan, B. Qu, J. Chen, H. Lv, X. Yang, Engineering modifiers bearing benzophenone with enhanced reactivity to construct surface microstructures, Polym. Chem. 10 (2019) 4859–4865, https://doi.org/10.1039/c9py00764d.
[31] Y. Iwasaki, S. Bunuasunthon, V.P. Hoven, Protein patterning with antifouling polymer gel platforms generated using visible light irradiation, Chem. Commun. 56 (2020) 5472–5475, https://doi.org/10.1039/d0cc02092c.
[32] O. Prucker, C.A. Naumann, J. Rühe, W. Knoll, C.W. Frank, Photochemical attachment of polymer films to solid surfaces via monolayers of benzophenone derivatives, J. Am. Chem. Soc. 121 (1999) 8766–8770, https://doi.org/10.1021/ja990962+.
[33] Q. Liu, J.L. Locklin, Photocross-linking kinetics study of benzophenone containing zwitterionic copolymers, ACS Omega 5 (2020) 9204–9211, https://doi.org/10.1021/acsomega.9b04493.
[34] K. Ishihara, K. Suzuki, Y. Inoue, K. Fukazawa, Effects of molecular architecture of photoreactive phospholipid polymer on adsorption and reaction on substrate surface under aqueous condition, J. Biomater. Sci. Polym. Ed. 32 (2020) 419–437, https://doi.org/10.1080/09205063.2020.1839340.
[35] J. Koc, E. Schönemann, R. Wanka, N. Aldred, A.S. Clare, H. Gardner, G.W. Swain, K. Hunsucker, A. Laschewsky, A. Rosenhahn, Effects of crosslink density in zwitterionic hydrogel coatings on their antifouling performance and susceptibility to silt uptake, Biofouling 36 (2020) 646–659, https://doi.org/10.1080/08927014.2020.1796983.
[36] M. Borgolte, O. Riester, T. Kacerova, S. Rentschler, M.S. Schmidt, S. Jacksch, M. Egert, S. Laufer, R. Csuk, H.P. Deigner, Methacryloyl-glcnac derivatives copolymerized with dimethacrylamide as a novel antibacterial and biocompatible coating, Pharmaceutics 13 (2021) 1647, https://doi.org/10.3390/pharmaceutics13101647.
[37] G. Dormán, H. Nakamura, A. Pulsipher, G.D. Prestwich, The life of pi star: exploring the exciting and forbidden worlds of the benzophenone photophore, Chem. Rev. 116 (2016) 15284–15398, https://doi.org/10.1021/acs.chemrev.6b00342.
[38] G. Dormán, G.D. Prestwich, Benzophenone photophores in biochemistry, Biochemistry 33 (1994) 5661–5673, https://doi.org/10.1021/bi00185a001.
[39] O. Prucker, T. Brandstetter, J. Rühe, Surface-attached hydrogel coatings via C,H-insertion crosslinking for biomedical and bioanalytical applications (Review), Biointerphases 13 (2018), 010801, https://doi.org/10.1116/1.4999786.
[40] M.M. Hassan, O.O. Olaoye, Recent advances in chemical biology using benzophenones and diazirines as radical precursors, Molecules 25 (2020) 2285, https://doi.org/10.3390/molecules25102285.
[41] H. Orelma, M. Vuoriluoto, L.S. Johansson, J.M. Campbell, I. Filpponen, M. Biesalski, O.J. Rojas, Preparation of photoreactive nanocellulosic materials: via benzophenone grafting, RSC Adv. 6 (2016) 85100–85106, https://doi.org/10.1039/c6ra15015b.
[42] G. Dormán, G.D. Prestwich, Benzophenone photophores in biochemistry, Biochemistry 33 (1994) 5661–5673, https://doi.org/10.1021/BI00185A001/ASSET/BI00185A001.FP.PNG_V03.
[43] M. Körner, O. Prucker, J. Rühe, Kinetics of the generation of surface-attached polymer networks through C, H-insertion reactions, Macromolecules 49 (2016) 2438–2447, https://doi.org/10.1021/acs.macromol.5b02734.
[44] M. Morimoto, T. Nakajima, M. Ishikura, Y. Shigemasa, S. Ifuku, H. Saimoto, Synthesis of organosoluble chitosan derivatives with polyphenolic side chains, Carbohydr. Polym. 90 (2012) 1259–1264, https://doi.org/10.1016/J.CARBPOL.2012.06.067.
[45] K.H. Hong, G. Sun, Antimicrobial and chemical detoxifying functions of cotton fabrics containing different benzophenone derivatives, Carbohydr. Polym. 71 (2008) 598–605, https://doi.org/10.1016/J.CARBPOL.2007.07.004.
[46] D. Garcia-Gonzalez, A. Rusinek, T. Jankowiak, A. Arias, Mechanical impact behavior of polyether–ether–ketone (PEEK), Compos. Struct. 124 (2015) 88–99, https://doi.org/10.1016/J.COMPSTRUCT.2014.12.061.
[47] S.M. Kurtz, J.N. Devine, PEEK biomaterials in trauma, orthopedic, and spinal implants, Biomaterials 28 (2007) 4845–4869, https://doi.org/10.1016/J.BIOMATERIALS.2007.07.013.
[48] A. Godara, D. Raabe, S. Green, The influence of sterilization processes on the micromechanical properties of carbon fiber-reinforced PEEK composites for bone implant applications, Acta Biomater. 3 (2007) 209–220, https://doi.org/10.1016/J.ACTBIO.2006.11.005.
[49] Lumbar interbody fusion using the brantigan I/F cage for pos... : Spine, (n.d.). https://journals.lww.com/spinejournal/Fulltext/2000/06010/Lumbar_Interbody_Fusion_Using_the_Brantigan_I_F.17.aspx (accessed 15, December 2021).
[50] D.-Y. Cho, W.-R. Liau, W.-Y. Lee, J.-T. Liu, C.-L. Chiu, P.-C. Sheu, Preliminary experience using a polyetheretherketone (PEEK) cage in the treatment of cervical disc disease, Neurosurgery 51 (2002) 1343–1350, https://doi.org/10.1227/01.NEU.0000309109.71345.19.
[51] J.W. Brantigan, A. Neidre, J.S. Toohey, The lumbar I/F cage for posterior lumbar interbody fusion with the variable screw placement system: 10-year results of a food and drug administration clinical trial, Spine J. 4 (2004) 681–688, https://doi.org/10.1016/J.SPINEE.2004.05.253.
[52] J.M. Toth, M. Wang, B.T. Estes, J.L. Scifert, H.B. Seim, A.S. Turner, Polyetheretherketone as a biomaterial for spinal applications, Biomaterials 27 (2006) 324–334, https://doi.org/10.1016/J.BIOMATERIALS.2005.07.011.
[53] A. Wang, R. Lin, C. Stark, J.H. Dumbleton, Suitability and limitations of carbon fiber reinforced PEEK composites as bearing surfaces for total joint replacements, Wear 225–229 (1999) 724–727, https://doi.org/10.1016/S0043-1648(99)00026-5.
[54] A Low Stiffness Composite Biologically Fixed Prosthesis : Clinical Orthopaedics and Related Research®, (n.d.). https://journals.lww.com/clinorthop/Fulltext/2001/12000/A_Low_Stiffness_Composite_Biologically_Fixed.15.aspx (accessed 15 December, 2021).
[55] S. Akhavan, M.M. Matthiesen, L. Schulte, T. Penoyar, M.J. Kraay, C.M. Rimnac, V.M. Goldberg, Clinical and histologic results related to a low-modulus composite total hip replacement stem, Journal of Bone and Joint Surgery - Series A 88 (2006) 1308–1314, https://doi.org/10.2106/JBJS.E.00316.
[56] F. el Halabi, J.F. Rodriguez, L. Rebolledo, E. Hurtós, M. Doblaré, Mechanical characterization and numerical simulation of polyether–ether–ketone (PEEK) cranial implants, J. Mech. Behav. Biomed. Mater. 4 (2011) 1819–1832, https://doi.org/10.1016/J.JMBBM.2011.05.039.
[57] S. Lovald, S.M. Kurtz, Applications of Polyetheretherketone in Trauma, Arthroscopy, and Cranial Defect Repair, PEEK Biomaterials Handbook, 2012, pp. 243–260, https://doi.org/10.1016/B978-1-4377-4463-7.10015-6.
[58] T.J. Hoskins, K.D. Dearn, S.N. Kukureka, Mechanical performance of PEEK produced by additive manufacturing, Polym. Test. 70 (2018) 511–519, https://doi.org/10.1016/J.POLYMERTESTING.2018.08.008.
[59] M. Rinaldi, T. Ghidini, F. Cecchini, A. Brandao, F. Nanni, Additive layer manufacturing of poly (ether ether ketone) via FDM, Compos. B Eng. 145 (2018) 162–172, https://doi.org/10.1016/J.COMPOSITESB.2018.03.029.
[60] B. Hu, X. Duan, Z. Xing, Z. Xu, C. Du, H. Zhou, R. Chen, B. Shan, Improved design of fused deposition modeling equipment for 3D printing of high-performance PEEK parts, Mech. Mater. 137 (2019), 103139, https://doi.org/10.1016/J.MECHMAT.2019.103139.
[61] S. Berretta, K. Evans, O. Ghita, Additive manufacture of PEEK cranial implants: manufacturing considerations versus accuracy and mechanical performance, Mater. Des. 139 (2018) 141–152, https://doi.org/10.1016/J.MATDES.2017.10.078.
[62] S. Najeeb, Z.K. Bds, S.Z. Bds, M.S.Z. Bds, Bioactivity and osseointegration of PEEK are inferior to those of titanium: a systematic review, J. Oral Implantol. 42 (2016) 512–516, https://doi.org/10.1563/aaid-joi-D-16-00072.
[63] F. Blendinger, D. Seitz, A. Ottenschläger, M. Fleischer, V. Bucher, Atomic layer deposition of bioactive TiO2 thin films on polyetheretherketone for orthopedic implants, ACS Appl. Mater. Interfaces 13 (2021) 3536–3546, https://doi.org/10.1021/ACSAMI.0C17990.
[64] A. Diouf-Lewis, R.D. Farahani, F. Iervolino, J. Pierre, Y. Abderrafai, M. Lévesque, N. Piccirelli, D. Therriault, Design and characterization of carbon fiber-reinforced PEEK/PEI blends for Fused Filament Fabrication additive

manufacturing, Mater. Today Commun. 31 (2022), 103445, https://doi.org/10.1016/J.MTCOMM.2022.103445.
[65] B.I. Oladapo, S.A. Zahedi, Improving bioactivity and strength of PEEK composite polymer for bone application, Mater. Chem. Phys. 266 (2021), 124485, https://doi.org/10.1016/J.MATCHEMPHYS.2021.124485.
[66] K. Hu, Z. Yang, Y. Zhao, Y. Wang, J. Luo, B. Tuo, H. Zhang, Bioinspired surface functionalization of poly(ether ether ketone) for enhancing osteogenesis and bacterial resistance, Langmuir 38 (2022) 5924–5933, https://doi.org/10.1021/ACS.LANGMUIR.2C00600/SUPPL_FILE/LA2C00600_SI_002.MP4.
[67] M. Kyomoto, K. Ishihara, Self-initiated surface graft polymerization of 2-methacryloyloxyethyl phosphorylcholine on poly(ether ether ketone) by photoirradiation, ACS Appl. Mater. Interfaces 1 (2009) 537–542, https://doi.org/10.1021/AM800260T/ASSET/IMAGES/MEDIUM/AM-2008-00260T_0005. GIF.
[68] M. Kyomoto, T. Moro, S. Yamane, M. Hashimoto, Y. Takatori, K. Ishihara, Poly(ether-ether-ketone) orthopedic bearing surface modified by self-initiated surface grafting of poly(2-methacryloyloxyethyl phosphorylcholine), Biomaterials 34 (2013) 7829–7839, https://doi.org/10.1016/J.BIOMATERIALS.2013.07.023.
[69] M. Kyomoto, T. Moro, Y. Takatori, H. Kawaguchi, K. Nakamura, K. Ishihara, Self-initiated surface grafting with poly(2-methacryloyloxyethyl phosphorylcholine) on poly(ether-ether-ketone), Biomaterials 31 (2010) 1017–1024, https://doi.org/10.1016/J.BIOMATERIALS.2009.10.055.
[70] C.J. Fristrup, K. Jankova, S. Hvilsted, Hydrophilization of poly(ether ether ketone) films by surface-initiated atom transfer radical polymerization, Polym. Chem. 1 (2010) 1696–1701, https://doi.org/10.1039/C0PY00142B.
[71] B. Yameen, M. Álvarez, O. Azzaroni, U. Jonas, W. Knoll, Tailoring of poly(ether ether ketone) surface properties via surface-initiated atom transfer radical polymerization, Langmuir 25 (2009) 6214–6220, https://doi.org/10.1021/LA900010Z/ASSET/IMAGES/MEDIUM/LA-2009-00010Z_0004. GIF.
[72] 87: Biological reactivity tests , in vitro, in: The United States Pharmacopeia. The National Formulary, United States Pharmacopeial Convention, Inc., Rockville, Md, 1979, pp. 92–94.
[73] E. Skyttä, T. Mattila-Sandholm, A quantitative method for assessing bacteriocins and other food antimicrobials by automated turbidimetery, J. Microbiol. Methods 14 (1991) 77–88, https://doi.org/10.1016/0167-7012(91)90036-P.
[74] Japan Food Research Laboratories, ISO, 2011, pp. 1–24. ISO 22196: Measurement of antibacterial activity on plastics and other non-porous surfaces.
[75] M.F. Queiroz, K.R.T. Melo, D.A. Sabry, G.L. Sassaki, H.A.O. Rocha, Does the use of chitosan contribute to oxalate kidney stone formation? Mar. Drugs 13 (2015) 141–158, https://doi.org/10.3390/MD13010141, 13 (2014) 141–158.
[76] Z.G. Tang, R.A. Black, J.M. Curran, J.A. Hunt, N.P. Rhodes, D.F. Williams, Surface properties and biocompatibility of solvent-cast poly[e-caprolactone] films, Biomaterials 25 (2004) 4741–4748, https://doi.org/10.1016/j.biomaterials.2003.12.003.
[77] ISO 10993-5:2009 Biological Evaluation of Medical Devices — Part 5: Tests for in Vitro Cytotoxicity, n.d.
[78] 88: biological reactivity tests , in vivo, in: The United States Pharmacopeia. The National Formulary, United States Pharmacopeial Convention, Inc., Rockville, Md, 1979, pp. 94–98.
[79] A.D. Baxter, R. Bhogal, J. Bird, J.F. Keily, D.T. Manallack, J.G. Montana, D.A. Owen, W.R. Pitt, R.J. Watson, R.E. Wills, Arylsulphonyl hydroxamic acids: potent and selective matrix metalloproteinase inhibitors, Bioorg. Med. Chem. Lett 11 (2001) 1465–1468, https://doi.org/10.1016/S0960-894X(01)00259-1.
[80] E.I. Heath, L.B. Grochow, Clinical potential of matrix metalloprotease inhibitors in cancer therapy, Drugs 59 (2000) 1043–1055, https://doi.org/10.2165/00003495-200059050-00002.
[81] S.B. Rodan, Y. Imai, M.A. Thiede, G. Wesolowski, D. Thompson, Z. Bar-Shavit, S. Shull, K. Mann, G.A. Rodan, Characterization of a human osteosarcoma cell line (Saos-2) with osteoblastic properties, Cancer Res. 47 (1987) 4961–4966.
[82] C. Sun, S. bin Feng, Z.W. Cao, J.J. Bei, Q. Chen, X.J. Xu, Z. Zhou, Z.P. Yu, H.Y. Hu, Up-regulated expression of matrix metalloproteinases in endothelial cells mediates platelet microvesicle-induced angiogenesis, Cell. Physiol. Biochem. 41 (2017) 2319–2332, https://doi.org/10.1159/000475651.
[83] T. Mori, M. Okumura, M. Matsuura, K. Ueno, S. Tokura, Y. Okamoto, S. Minami, T. Fujinaga, Effects of chitin and its derivatives on the proliferation and cytokine production of fibroblasts in vitro, Biomaterials 18 (1997) 947–951, https://doi.org/10.1016/S0142-9612(97)00017-3.
[84] J. Brown, Using the monocyte activation test as a stand-alone release test for medical devices, ALTEX (2021) 151–156, https://doi.org/10.14573/altex.2012021.
[85] Y. Nakagawa, H. Maeda, T. Murai, Evaluation of the in vitro pyrogen test system based on proinflammatory cytokine release from human monocytes: comparison with a human whole blood culture test system and with the rabbit pyrogen test, Clin. Diagn. Lab. Immunol. 9 (2002) 588–597, https://doi.org/10.1128/CDLI.9.3.588-597.2002.
[86] Y.v. Chaly, R.S. Selvan, K.v. Fegeding, T.S. Kolesnikova, N.N. Voitenok, Expression of IL-8 gene in human monocytes and lymphocytes: differential regulation by tnf and IL-1, Cytokine 12 (2000) 636–643, https://doi.org/10.1006/CYTO.1999.0664.
[87] H.-Y. Hsu, M.-H. Wen, Lipopolysaccharide-mediated reactive oxygen species and signal transduction in the regulation of interleukin-1 gene expression, J. Biol. Chem. 277 (2002) 22131–22139, https://doi.org/10.1074/jbc.M111883200.
[88] H. Yuan, C.N. Perry, C. Huang, E. Iwai-Kanai, R.S. Carreira, C.C. Glembotski, R.A. Gottlieb, LPS-induced autophagy is mediated by oxidative signaling in cardiomyocytes and is associated with cryoprotection, Am. J. Physiol. Heart Circ. Physiol. (2009) 296, https://doi.org/10.1152/AJPHEART.01051.2008/ASSET/IMAGES/LARGE/ZH40030987000009. JPEG.
[89] J.G. Gray, G. Chandra, W.C. Clay, S.W. Stinnett, S.A. Haneline, J.J. Lorenz, I.R. Patel, G. Bruce Wisely, P.J. Furdon, J.D. Taylor, T.A. Kost', A CRE/ATF-like site in the upstream regulatory sequence of the human interleukin 1 beta gene is necessary for induction in U937 and THP-1 monocytic cell lines, Mol. Cell Biol. 13 (1993) 6678–6689, https://doi.org/10.1128/MCB.13.11.6678-6689.1993.
[90] K. Li, R. Xing, S. Liu, R. Li, Y. Qin, X. Meng, P. Li, Separation of chito-oligomers with several degrees of polymerization and study of their antioxidant activity, Carbohydr. Polym. 88 (2012) 896–903, https://doi.org/10.1016/j.carbpol.2012.01.033.
[91] H. Anggani, E. Hasriati, E. Winiati Bachtiar, Evaluation of IL-1α and IL-1β, COX-2, and iNOS mRNA expression in orthodontic patients given chitosan mouthwash during treatment with miniscrew, J. Int. Soc. Prev. Community Dent. 11 (2021) 561–565, https://doi.org/10.4103/JISPCD.JISPCD_163_21.
[92] T.-C. Chou, E. Fu, E.-C. Shen, Chitosan inhibits prostaglandin E2 formation and cyclooxygenase-2 induction in lipopolysaccharide-treated RAW 264.7 macrophages, Biochem. Biophys. Res. Commun. 308 (2003) 403–407, https://doi.org/10.1016/S0006-291X(03)01407-4.
[93] G.-W. Oh, S.-C. Ko, J.-Y. Je, Y.-M. Kim, J. Oh, W.-K. Jung, Fabrication, characterization and determination of biological activities of poly(ε-caprolactone)/chitosan-caffeic acid composite fibrous mat for wound dressing application, Int. J. Biol. Macromol. 93 (2016) 1549–1558, https://doi.org/10.1016/j.ijbiomac.2016.06.065.
[94] M. Valko, K. Jomova, C.J. Rhodes, K. Kuča, K. Musílek, Redox- and Non-redox-metal-induced Formation of Free Radicals and Their Role in Human Disease, 2016, https://doi.org/10.1007/s00204-015-1579-5.
[95] Z. Li, F. Yang, R. Yang, Synthesis and characterization of chitosan derivatives with dual-antibacterial functional groups, Int. J. Biol. Macromol. 75 (2015) 378–387, https://doi.org/10.1016/J.IJBIOMAC.2015.01.056.
[96] L. Hu, X. Meng, R. Xing, S. Liu, X. Chen, Y. Qin, H. Yu, P. Li, Design, synthesis and antimicrobial activity of 6-N-substituted chitosan derivatives, Bioorg. Med. Chem. Lett 26 (2016) 4548–4551, https://doi.org/10.1016/J.BMCL.2015.08.047.
[97] H. Liu, P. Sun, H. Liu, S. Yang, L. Wang, Z. Wang, Acute toxicity of benzophenone-type UV filters for Photobacterium phosphoreum and Daphnia magna: QSAR analysis, interspecies relationship and integrated assessment, Chemosphere 135 (2015) 182–188, https://doi.org/10.1016/J.CHEMOSPHERE.2015.04.036.
[98] A.K. Refai, M. Textor, D.M. Brunette, J.D. Waterfield, Effect of titanium surface topography on macrophage activation and secretion of proinflammatory cytokines and chemokines, J. Biomed. Mater. Res. 70A (2004) 194–205, https://doi.org/10.1002/jbm.a.30075.